Journal of Alloys and Compounds 588 (2014) 75–95

Contents lists available at ScienceDirect

Journal of Alloys and Compounds

journal homepage: www.elsevier.com/locate/jalcom

Experimental and thermodynamic study of the Mg–Sn–In–Zn quaternary system

Jian Wang [a], Pierre Hudon [b], Dmytro Kevorkov [c], Patrice Chartrand [a,*], In-Ho Jung [b], Mamoun Medraj [c]

[a] Center for Research in Computational Thermochemistry (CRCT), Department of Chemical Engineering, École Polytechnique, Montréal, Quebec H3C 3A7, Canada
[b] Department of Mining and Materials Engineering, McGill University, 3610 University Street, Montreal, Quebec H3A 0C5, Canada
[c] Department of Mechanical Engineering, Concordia University, 1455 De Maisonneuve Blvd. West, Montreal, Quebec H3G 1M8, Canada

ARTICLE INFO

Article history:
Received 3 September 2013
Received in revised form 17 October 2013
Accepted 6 November 2013
Available online 14 November 2013

Keywords:
Metals and alloys
Phase diagram
Thermodynamic modeling
Electron probe micro-analyzer
SEM

ABSTRACT

Phase equilibria in the Mg-rich region of the Mg–Sn–In (at 415 °C and 330 °C), and Mg–Sn–Zn (at 300 °C) ternary systems were determined by quenching experiments, electron probe micro-analyzer (EPMA), and X-ray diffraction (XRD) techniques. The ternary isoplethal sections with constant 5 In and 10 Sn at.% of Mg–In–Sn system, and 10 Sn at.% of Mg–In–Zn system were determined by differential scanning calorimetry (DSC). No ternary compounds were found in the Mg–Sn–Zn and Mg–Sn–In isothermal sections. Critical evaluation and thermodynamic optimization of the Mg–Sn–In–Zn quaternary system were carried out using CALPHAD (Calculation of Phase Diagrams) technique. The Modified Quasichemical Model in the Pair Approximation (MQMPA) was used for modeling the liquid solution, which exhibits a high degree of short-range ordering behavior. The solid phases were modeled with the Compound Energy Formalism (CEF). All available and reliable experimental data were reproduced within experimental error limits. A self-consistent thermodynamic database was constructed for the Mg–Sn–In–Zn quaternary system, which can be used as a guide for Mg-based alloys development.

1. Introduction

Magnesium-based alloys are very attractive to the automotive and aeronautic industries thanks to their low density (approximately 1.80 g/cm^3), which is lower than Al based alloys (~2.80 g/cm^3) and steels (~7.90 g/cm^3). In addition, Mg-based alloys have good processing properties and are almost completely recyclable [1,2]. Up to now, several series of magnesium alloys were developed, which includes the Mg–Al, Mg–Mn, Mg-Rare-Earths, and Mg–Zn series. The Mg–Zn series is the first hardenable Mg-based alloy developed for structural materials. The high solid solubility of Zn in Mg (hcp) phase and the considerable amount of secondary precipitates in the Mg matrix can produce a very good age-hardening effect [3]. Unfortunately, the Mg–Zn series has the same problem than the Mg–Al series (but the AE series), that is poor mechanical properties at elevated temperature which restricts its applications. On the other hand, Mg–Sn based alloys have stable microstructures and good mechanical properties at high temperature due to the high solubility of Sn in Mg (hcp) and the potential to precipitate a cubic structure second phase (Mg_2Sn) in the magnesium-rich matrix [4,5]. Moreover, the solubility of Sn in Mg (hcp) drops sharply from about 15 wt.% at 561 °C to 0.45 at 200 °C, which provides the wide heat treatment temperature range necessary to obtain good mechanical properties through ageing process. Unfortunately, Mg–Sn alloys require quite long ageing times to reach peak hardness, which is not practical for industrial applications [6]. In addition to Sn, another element, In, is also known to improve the mechanical properties of Mg-based alloys. According to Mendis et al. [7,8], and Becerra and Pekguleryuz [9], indium is quite beneficial to the mechanical properties of Mg based alloys. In brief, Zn, Sn, and In are good candidates to develop new Mg-based alloys but up to now, experimental research on the Mg–Zn–Sn–In quaternary system and especially the effects associated to the addition of In to Mg–Zn–Sn ternary alloys, is quite limited.

Obtaining phase equilibrium information by the sole mean of experimental techniques is cumbersome and costly. Fortunately, thermodynamic modeling of multi-component systems by the CALPHAD (Calculation of Phase Diagrams) [10] approach has proven to be a very efficient way to investigate and develop new alloys [11]. In order to obtain Mg–Sn–In–Zn alloys with good mechanical properties at high temperatures and better understand the relationships existing between phase equilibria and alloy microstructures, the thermodynamic database of the Mg–Sn–In–Zn system was constructed in the present work experimentally and thermodynamically.

* Corresponding author. Tel.: +1 514 340 4711x4089; fax: +1 514 340 5840.
E-mail address: patrice.chartrand@polymtl.ca (P. Chartrand).

0925-8388/$ - see front matter © 2013 Elsevier B.V. All rights reserved.
http://dx.doi.org/10.1016/j.jallcom.2013.11.031

Table 1
Optimized phases and thermodynamic models used in the present work.

Phase	Pearson symbol	Strukturbericht designation	Space group	Prototype	Model[a]
Liquid	–	–	–	–	MQMPA
fcc	cF4	A1	$Fm\bar{3}m$	Cu	CEF
bct	tI4	A5	$I4_1/mmm$	Sn	CEF
bcc	cI2	A2	$Im\bar{3}m$	W	CEF
hcp	hP2	A3	$P6_3/mmc$	Mg	CEF
hcp (Zn)	hP2	A3	$P6_3/mmc$	Mg	CEF
tet	tI2	A6	$F4/mmm$	In	CEF
β'	cP4	$L1_2$	$F4/mmm$	$AuCu_3$	CEF
β_1	hR16	–	$R3m$	–	CEF
β_2	hP9	–	$P\bar{6}2m$	Mg_2Tl	ST
β_3	oI28	$D8_g$	$Ibam$	Mg_5Ga_2	ST
β''	tP4	$L1_0$	$P4/mmm$	AuCu	CEF
γ'	cP4	$L1_2$	$Pm3m$	$AuCu_3$	CEF
$Mg_{12}Zn_{13}$	–	–	–	–	ST
Mg_2Zn_3	mC110	–	$B2/m$	–	ST
$MgZn_2$	hP12	C14	$P6_3/mmc$	$MgZn_2$	ST
Mg_2Zn_{11}	cP39	$D8_c$	$Pm\bar{3}$	Mg_2Zn_{11}	ST
$Mg_{51}Zn_{20}$	oI142	$D7_b$	$Immm$	Ta_3B_4	ST
Mg_2Sn	cF12	C1	$Fm\bar{3}m$	CaF_2	ST
β(InSn)	tI2	A6	$F4/mmm$	In	CEF
γ(InSn)	hP5	–	$P6/mmm$	–	CEF

[a] MQMPA: Modified Quasichemical Model in the Pair Approximation; CEF: Compound Energy Formalism; ST: Stoichiometric Compound.

2. Literature review

2.1. The In–Mg systems

Phase equilibria in the Mg-rich portion (0–20 at.% In) of the In–Mg binary system was first studied by Hume-Rothery and Raynor [12] by means of thermal analysis and metallographic observation methods. The liquidus and solidus curves were determined and a large solid solution field located between 18.6 and 19.4 at.% In in the Mg (hcp) phase was reported. The whole composition range of the In–Mg binary system was examined by Hancke [13] by using XRD; four intermediate phases were reported: Mg_5In_2 (body-centered rhombic), Mg_2In (hexagonal), MgIn (body-centered tetragonal) and $MgIn_3$. Later, the constitution of In–Mg alloys between 20 and 50 at.% In was studied by Raynor [14] by using optical microscopy, electrolytic measurements, and XRD. The peritectic reaction *liquid + Mg (hcp)* $\leftrightarrow \beta$ was found to occur at 302 °C at a liquid composition of 23.2 at.% In. Two intermediate phases, β_1 and β_2, were found, and the solubility in β_1 was found to lie between 23.5 and 25 at.% In. Raynor [14] also found that β_1 and β_2 have very complex crystal structures, and noted that the crystal structure of β_1 is different from that of Mg_5In_2 [13]). Moreover, Raynor [14] pointed out that β_2 may actually correspond to Mg_2In, as reported earlier by Hancke [13]. Two ordering transformations, $\beta \rightarrow \beta'(L1_2)$, and $\beta \rightarrow \beta''(L1_0)$, are mentioned in Raynor's work [14]. Graham and Raynor [15] investigated several In–Mg binary alloys by using XRD and metallography, and the peritectic reaction *fcc + liquid* $\leftrightarrow$ *tet(In)* was found to occur at 333.5 °C. Ino et al. [16] investigated the ordering phase transformation in the In–Mg system between 36.8 and 56.3 at.% In using XRD and thermal analysis. According to them, the $\beta \rightarrow \beta'(L1_2)$ and $\beta \rightarrow \beta''(L1_0)$ transformations go through two phase regions of $\beta + \beta'(L1_2)$ and $\beta + \beta''(L1_0)$, respectively. Phase equilibria in the In–Mg binary system was afterwards investigated up to 40 at.% Mg by Hiraga et al. [17] by using XRD, thermal analysis, and calorimetry. The solid solubility of magnesium in indium was found to reach about 5 at.%. The peritectic reaction *fcc + liquid* $\leftrightarrow$ *tet(In)* was reported to occur at 160 °C by Hiraga et al. [17], which is quite different from the temperature observed earlier by Graham and Raynor (333.5 °C) [15]. In the In-rich portion, a new ordered phase, γ', with a Cu_3Au-type structure, was reported by Hiraga et al. [17] based on thermal and X-ray analysis. The In-rich region was reinvestigated by Pickwick et al. [18] and Feschotte [19] by using differential thermal analysis (DTA), electrical resistivity measurements, and metallographic observation methods. The temperatures of the peritectic reactions *liquid + hcp(Mg)* $\leftrightarrow \beta$ and *fcc + liquid* $\leftrightarrow$ *tet(In)* were observed to occur at 305 ± 0.5 °C and 160 °C, respectively, which is in good agreement with the data of Hiraga et al. [17]. Pickwick et al. [18] also observed that the intermediate fcc solid solution is homogeneous over a wide range, from 23 to 86 at.% In. Watanabe [20] re-examined the In–Mg system near the Mg_3In composition and the β_3 phase, reported as Mg_5In_2 in Hancke's work [13], was confirmed. According to Watanabe [20], the β_3 phase is only stable below 210 °C and decomposes to β' and β_2 above this temperature. The whole thermodynamic and phase equilibra data of the In–Mg binary system were compiled by Nayeb-Hashemi and Clark [21]. Seven binary compounds were considered: β, β_1, β_2, β_3, β', β'' and γ', where β' and γ' are ordered phases with the fcc $L1_2$ structure ($AuCu_3$), and β'' is another ordered fcc phase with the $L1_0$ structure ($AuCu$).

The thermodynamic properties of activities of In and Mg, enthalpy and entropy mixing of the In–Mg liquid phase were studied by calorimetric measurements [22,23], EMF measurements [23–27], and vapour pressure measurements [28]. Ehrlich [22] reported the experimental enthalpy of mixing of the In–Mg liquid phase at 650 °C using direct calorimetric measurements. Moser and Castanet [23,27] studied the In–Mg liquid solution by an EMF technique based on the concentration cell: $Mg_{(s)}$//($MgCl_2$–$LiCl$–KCl)//Mg–$In_{(liq.)}$. And the activities, enthalpy mixing and Gibbs energy of mixing at 577 °C were derived in their work [23,27] based on the results from EMF measurements. Slaby and Terpilowski [24,25] investigated the Mg–In liquid phase using EMF measurements with the type of cell: $Mg_{(s)}$//(*0.58LiCl + 0.42KCl + 0.05*$MgBr_2$)//Mg_xIn_{1-x}. The enthalpy of mixing, entropy of mixing, and the activity of In and Mg in the liquid phase at 650 °C were extrapolated by Slaby and Terpilowski [24,25] based on their

Table 2
Optimized binary model parameters of the MQMPA for the Mg–Sn–In–Zn liquid solution.

Coordination numbers[a]				Gibbs energies of pair exchange reactions (J/mol-atoms)	Reference
i	j	Z^i_{ij}	Z^j_{ij}		
Mg	In	3	6	$\Delta g_{Mg,In} = -9790.6 - 2092X_{InIn} - 209.2X^2_{InIn}$	This work
Mg	Sn	4	8	$\Delta g_{Mg,Sn} = -15263.2 - 0.88 \times T + (3347.2 + 0.42 \times T)X_{MgMg}$	[85]
Mg	Zn	6	6	$\Delta g_{Mg,Zn} = -6778.1 + 3.14 \times T - (1966.5 - 2.01 \times T)X_{MgMg} - (3974.8 - 1.67 \times T)X_{ZnZn}$	[86]
In	Zn	6	4	$\Delta g_{In,Zn} = 5104.5 - 2.22 \times T + (962.3 - 0.71 \times T)X_{ZnZn}$	This work
In	Sn	6	6	$\Delta g_{In,Sn} = -175.7 - 138.1X_{InIn} - 133.9X_{SnSn}$	This work
Sn	Zn	6	6	$\Delta g_{Sn,Zn} = 2259.4 + (2175.7 - 4.18 \times T)X_{SnSn} + (5355.5 - 5.86 \times T)X_{ZnZn}$	[73]

Note: T in K.
[a] For all pure elements (Mg, Li, and Sn), $Z^i_{ii} = 6$.

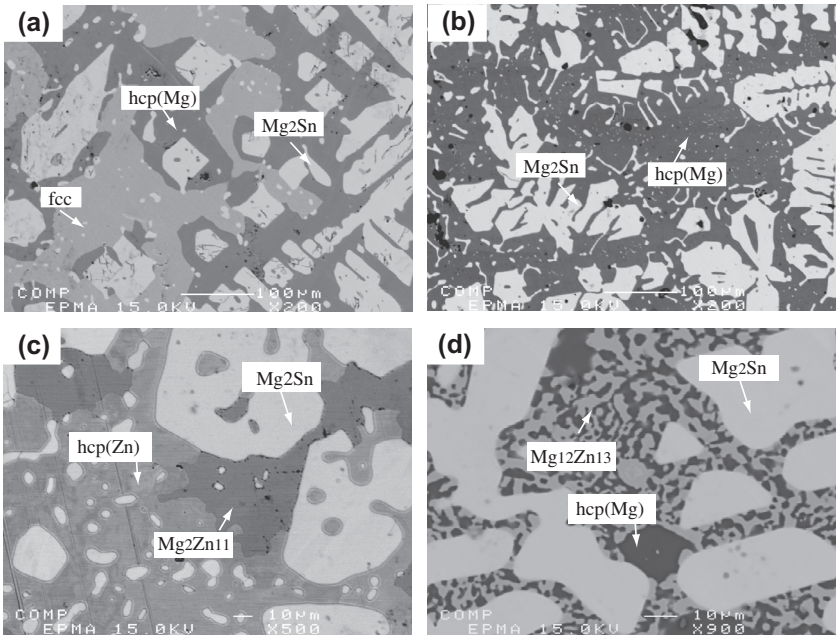

Fig. 1. Typical ternary BSE images obtained from (a) Mg78Sn10In12 (at.%) alloy annealed at 415 °C for 20 days; (b) Mg80Sn10In10 (at.%) alloy annealed at 330 °C for 35 days; (c) Mg25Sn10Zn65 (at.%) alloy annealed at 300 °C for 50 days; (d) Mg70Sn10Zn20 (at.%) alloy annealed at 300 °C for 50 days.

Table 3
Equilibrium compositions in the Mg–Sn–X (X: In, Zn) ternary systems as measured in the present work.

System	Temp. (°C)	Alloy nominal comp. (at.%)	Phase equilibira	Composition (at.%)								
			Phase 1/Phase 2/Phase 3	Phase 1			Phase 2			Phase 3		
				Mg	Sn	In	Mg	Sn	In	Mg	Sn	In
Mg–Sn–In	415	Mg80Sn10In10	hcp(Mg)/Mg_2Sn/–	84.77	0.39	14.84	67.81	31.91	0.28	–	–	–
		Mg78Sn10In12	hcp(Mg)/Mg_2Sn/fcc	80.55	0.34	19.11	67.82	31.79	0.39	77.73	0.15	22.12
		Mg70Sn10In20	Mg_2Sn/fcc/–	67.32	32.26	0.42	70.34	0.35	29.31	–	–	–
		Mg65Sn10In25	Mg_2Sn/fcc/–	67.30	32.50	0.20	64.07	0.15	35.78	–	–	–
	330	Mg80Sn10In10	hcp(Mg)/Mg_2Sn/–	84.73	0.15	15.12	67.76	31.93	0.31	–	–	–
		Mg78Sn10In12	hcp(Mg)/Mg_2Sn/β_1	81.59	0.10	18.31	67.50	32.15	0.35	75.11	0.38	24.51
		Mg70Sn10In20	Mg_2Sn/$\beta(L1_2)$/–	67.83	31.87	0.30	70.92	0.13	28.95	–	–	–
		Mg65Sn10In25	Mg_2Sn/fcc/–	67.68	31.96	0.36	62.53	0.15	37.32	–	–	–
				Mg	Sn	Zn	Mg	Sn	Zn	Mg	Sn	Zn
Mg–Sn–Zn	300	Mg70Sn10Zn20	hcp (Mg)/Mg_2Sn/$Mg_{12}Zn_{13}$	98.00	0.23	1.77	67.95	32.02	0.03	50.44	0.6	48.96
		Mg50Sn10Zn40	Mg_2Sn/Mg_2Zn_3/$Mg_{12}Zn_{13}$	67.42	32.46	0.12	42.73	0.02	57.25	50.80	0.04	49.16
		Mg45Sn10Zn45	Mg_2Sn/Mg_2Zn_3/–	67.87	32.09	0.04	38.99	3.17	57.84	–	–	–
		Mg25Sn10Zn65	Mg_2Sn/Mg_2Zn_{11}/hcp(Zn)	67.09	32.84	0.07	18.90	3.98	77.12	0.95	1. 5	97.55

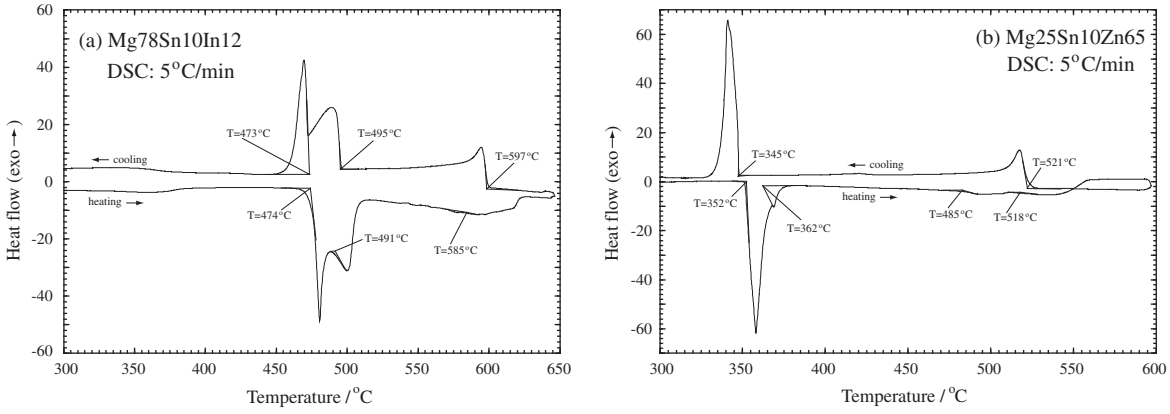

Fig. 2. The DSC curves of (a) Mg78Sn10In12 and (b) Mg25Sn10Zn65 alloys obtained in the present work.

Table 4
Thermal signals obtained from DSC measurements with the corresponding interpretation from the thermodynamic calculations for the Mg–Sn–In ternary system.

System	Alloy nominal comp. (at.%)	Thermal signals (°C)		Interpretation	
		Heating	Cooling	Calculated phase boundary or invariant reaction with temp. (°C)	
Mg–Sn–In	Mg80Sn10In10	596	592	583	liquid/liquid + Mg_2Sn
		524	513	533	liquid + Mg_2Sn/liquid + Mg_2Sn + hcp
		473	471	474	liquid + hcp ↔ Mg_2Sn + fcc
	Mg78Sn10In12	585	597	591	liquid/liquid + Mg_2Sn
		491	495	521	liquid + Mg_2Sn/liquid + Mg_2Sn + hcp
		474	473	474	liquid + hcp ↔ Mg_2Sn + fcc
	Mg70Sn10In20	614	614	608	liquid/liquid + Mg_2Sn
		448	452	463	liquid + Mg_2Sn/liquid + Mg_2Sn + fcc
		359	373	359	Mg_2Sn + fcc/Mg_2Sn + β'
	Mg65Sn10In25	596	604	607	liquid/liquid + Mg_2Sn
		389	397	427	liquid + Mg_2Sn/liquid + Mg_2Sn + fcc
		326	324	329	Mg_2Sn + fcc/Mg_2Sn + β' + *fcc*
	Mg90Sn5In5	572	558	592	liquid/liquid + hcp
		539	537	552	liquid + hcp/liquid + Mg_2Sn
	Mg85Sn10In5	584	580	563	liquid/liquid + Mg_2Sn
		532	542	541	liquid + Mg_2Sn + hcp/hcp + Mg_2Sn
	Mg40Sn55In5	490	480	557	liquid/liquid + Mg_2Sn
		193	185	185	liquid + Mg_2Sn/liquid + Mg_2Sn + γ(InSn)
		182	–	172	liquid + Mg_2Sn + γ(InSn)/Mg_2Sn + γ(InSn)
Mg–Sn–Zn	Mg50Sn10Zn40	–	616	608	liquid/liquid + Mg_2Sn
		524	543	553	liquid + Mg_2Sn/liquid + Mg_2Sn + $MgZn_2$
		399	–	413	liquid + Mg_2Sn + $MgZn_2$/liquid + Mg_2Zn_3 + Mg_2Sn
		343	348	350	liquid + Mg_2Zn_3 + Mg_2Sn/Mg_2Zn_3 + Mg_2Sn + $Mg_{12}Zn_{13}$
	Mg45Sn10Zn45	–	624	604	liquid/liquid + Mg_2Sn
		558	562	565	liquid + Mg_2Sn/liquid + Mg_2Sn + $MgZn_2$
	Mg35Sn10Zn55	542	564	575	liquid/liquid + Mg_2Sn
		344	352	357	liquid + $MgZn_2$ ↔ Mg_2Zn_{11} + Mg_2Sn
		337	332		–
	Mg25Sn10Zn65	518	521	509	liquid/liquid + Mg_2Sn
		485	–	480	liquid + Mg_2Sn/liquid + Mg_2Sn + $MgZn_2$
		362	–	–	–
		352	345	357	liquid + $MgZn_2$ ↔ Mg_2Zn_{11} + Mg_2Sn

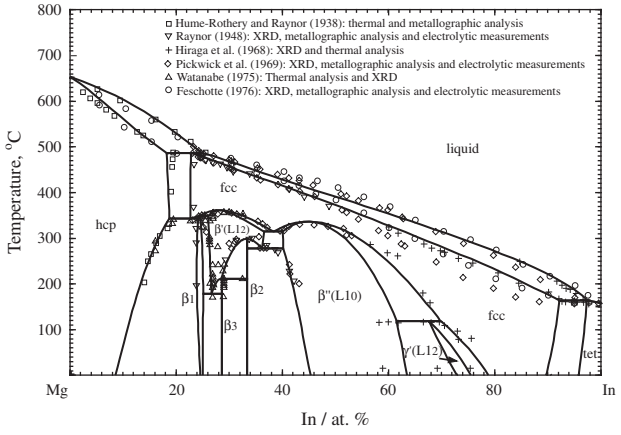

Fig. 3. Calculated Mg–In binary phase diagram compared with the reported experimental data [12,14,17–20].

measurements obtained from EMF techniques. Nebell [26] studied the In–Mg liquid phase in the temperature range from 450 °C to 650 °C by measuring the EMF of the galvanic cells: $Mg_{(s)}//(MgF_2$–$LiCl$–$KCl)//Mg$–$In_{(liq.)}$ and derived the enthalpy and entropy mixing properties. The enthalpy mixing results at 650 °C reported by Nebell [26] are in good agreement with the results reported by Moser and Castanet [23,27], but more positive (about 2 kJ/mol at 60 at.% Mg) than the data from Slaby and Terpilowski [24,25]. Chirulli et al. [28] investigated the activity of Mg in the liquid phase at 627 °C by using a torsion–effusion apparatus. Moser and Castanet [27] reported the experimental enthalpy of mixing of the In–Mg liquid phase at 650 °C, 675 °C and 735 °C using direct calorimetric measurements, their results are in good agreement with each other, but a little bit more positive than the data reported by Slaby and Terpilowski [24,25] and a bit more negative than the data reported by Nebell [26] and Moser and Castanet [23].

Thermodynamic optimization of the Mg–In binary system was not carried out previously. Consequently, the Mg–In binary system was optimized in the present work for the first time.

2.2. The In–Sn system

The phase diagram of the In–Sn binary system has been investigated by several authors [29–36]. The present accepted phase diagram, constituted with two intermetallic phases, β(InSn) and γ(InSn), plus the bct(Sn) and tet(In) terminal solid solution, is compiled mainly from the reported results of Heumann and Alpaut [34] who used differential thermal analysis (DTA), X-ray, dilatometric measurements and microscopic observations, and the reported results of Cakir and Alpaut [35] who used EMF measurements. The liquidus curve was determined by Heumann and Alpaut [34] using DTA measurements. Two peritectic reactions *liquid* + *tet* ↔ $\beta(InSn)$ *and* *liquid* + *bct* ↔ $\gamma(InSn)$ and one eutectic reaction *liquid* ↔ $\gamma(InSn)$ + $\beta(InSn)$ were reported with at 143 °C, 224 °C and 120 °C respectively [34]. Predel and Godecke [29] determined the phase equilibria in the Sn-rich region with DTA measurements. The phase diagram of the In–Sn binary system in the whole composition range was determined by Evans and Prince [30] using DTA measurements. Kaplun [31] determined the phase equilibria in the composition range from 0 to 60 Sn (at.%) using thermal analysis. The solid phases were determined by Wojtaszek and Kuzyk [32,33] using electrical resistance ratio measurements. All the reported experimental data show a reasonable agreement.

Table 5
The calculated results of invariant reactions in the In–Mg system compared with experimental data.

Reaction	Reaction type	Temperature (°C)	Composition (In at.%)			Reference
liquid + hcp ↔ *fcc*	Peritectic	484	25	19.4	23	[29,32–33]
		483	24.8	18.3	22.7	This work
fcc ↔ β_1 + *hcp*	Eutectoid	334	23.2	19	24	[35]
		335	22.4	18.4	24	This work
liquid + *fcc* ↔ *tet*	Peritectic	160 ± 1	97	93.5	95	[32]
		160	96.5	86	94	[33]
		161	97.8	92.5	97.4	This work
fcc + β' ↔ β_1	Peritectiod	337	23.9	26	24.4	[35]
		340	23.5	25.7	24.3	This work
β' ↔ β_1 + β_3	Eutectoid	202	27.5	26.2	28.6	[35,86]
		167	26.4	25.1	28.6	This work
β' + β_2 ↔ β_3	Peritectoid	210	27.6	33.8	28.6	[35]
		211	28.1	33.3	28.5	This work
β' ↔ β_2	Congruent	298		34		[29,35]
		298		33.3		This work
β' ↔ β_2 + β''	Eutectoid	276	37.8	33.5	38.2	[31]
		281	36	33.3	40	This work
β'' + *fcc* ↔ γ'	Peritectoid	114	58.5	70	69.5	[32]
		111	60.5	67.3	69.5	This work

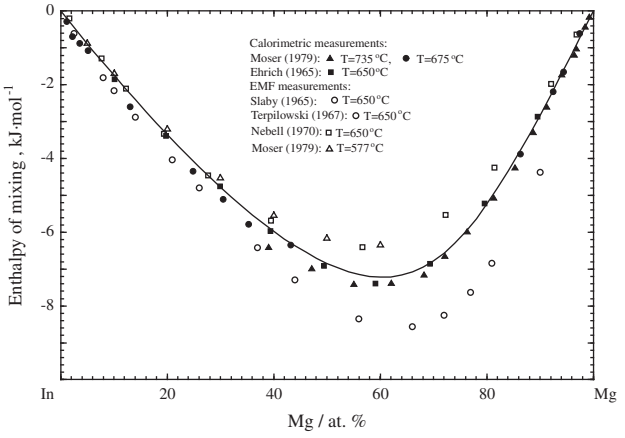

Fig. 4. Calculated enthalpy of mixing of the In–Mg liquid phase at 675 °C in comparison with the reported experimental data [22–27].

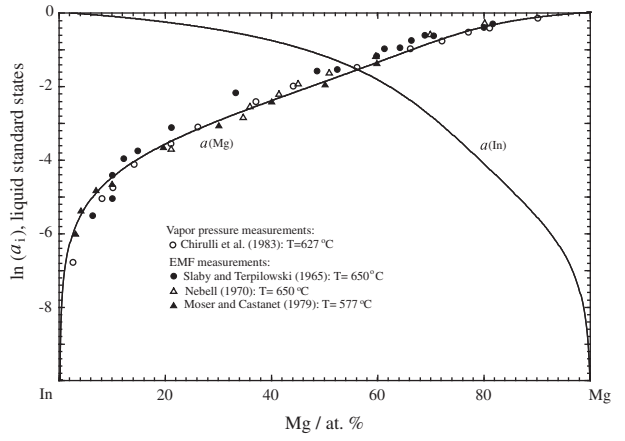

Fig. 5. Calculated activities of Mg and In in the liquid phase at 650 °C in comparison with the reported experimental data [24,26–28].

Activity data for In and Sn in the In–Sn liquid phase at different temperatures have been determined by Vassiliev et al. [37], Heumann and Alpaut [34], Terpilowski and Prezdziecka-Mycielska [38] using EMF techniques. Zivkovic et al. [39] investigated the activities of In and Sn in the In–Sn liquid phase at 327 °C using

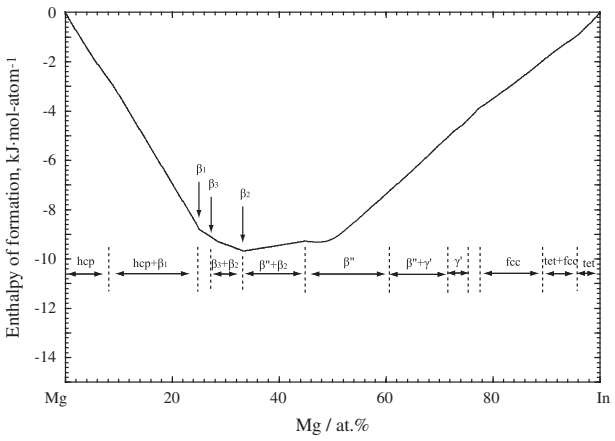

Fig. 6. Calculated enthalpy of formation of solid phases of the In–Mg binary system 25 °C.

Oelsen calorimetry. The enthalpy of mixing of the liquid phase was determined with a calorimetric method by Wittig and Scheidt [40], Kleppa [41], Yazawa et al. [42], Bros and Laffitte [43], Rechchach et al. [44] in the temperature range from 248 °C to 500 °C. Their results are in a reasonable agreement with the experimental error bar of ±10 J/mol. The enthalpy of formation and activity of In in the solid phases for the temperature range from 75 °C to 125 °C were determined by Cakir and Alpaut [35] using EMF measurements, and by Alpaut and Heumann [45] using quantitative thermal analysis, respectively.

The In–Sn binary system was optimized by Lee et al. [36] with Bragg-Williams ideal mixing modeling (BWM) for liquid phase in 1997, their optimization are in good agreement with the reported experimental data at that time. In order to construct a self-consistent thermodynamic database of Mg–Sn–In–Zn quaternary system, the In–Sn system was re-optimized with the Modified Quasichemical Model in the Pair Approximation (MQMPA) [46,47] for liquid phase, and with the recently reported experimental data in the present work.

2.3. In–Zn system

Experimental phase equilibrium and thermodynamic data of the In–Zn system were evaluated and compiled by Dutkiewicz

Table 6
Optimized thermodynamic parameters for the quaternary Mg–Sn–In–Zn system.

Phase, model and thermodynamic parameters (J mol^{-1}, or J mol^{-1} K^{-1})	Reference
Liquid phase, MQMPA	
$g^{001}_{InSn(Mg)} = -9204.8$,	This work
$g^{001}_{InSn(Zn)} = -2928.8,\ g^{001}_{InZn(Sn)} = 1255.2,\ g^{001}_{ZnSn(In)} = 1255.2$	This work
$g^{001}_{MgSn(Zn)} = -3765.6 + 3.14 \times T,\ g^{001}_{MgZn(Sn)} = -5439.2 + 2.30 \times T,\ g^{001}_{ZnSn(Mg)} = -1255.2 + 2.72 \times T$	This work
$hcp_{A3}(Mg)$ *phase* $(In, Mg, Sn, Zn)(Va)_3$	
$G_{Mg:Va} = {}^0G^{hcp}_{Mg},\ G_{Zn:Va} = {}^0G^{hcp_{Zn}}_{Zn} + 2969.0 - 1.57 \times T$	This work
$G_{Sn:Va} = {}^*G_{Sn} + 3900.0 - 4.4 \times T, G_{In:Va} = {}^*G_{In} + 533.0 - 0.69 \times T,$	[85]
${}^1L_{Mg,Sn:Va} = 48116.0,$	This work
${}^0L_{In,Zn:Va} = 6945.4,\ {}^0L_{Mg,In:Va} = -28325.7 + 6.07 \times T, {}^1L_{Mg,In:Va} = -10460.0 + 5.44 \times T$	
fcc_{A1} *phase* $(In, Mg, Sn, Zn)(Va)_3$	
$G_{Mg:Va} = {}^0G^{hcp}_{Mg} + 2600.0 + 0.90 \times T, G_{Zn:Va} = {}^0G^{hcp\_Zn}_{Zn} + 2969.0 + 1.57 \times T$	
$G_{In:Va} = {}^*G_{In} + 123.0 - 0.30 \times T, G_{Sn:Va} = {}^*G_{Sn} + 4150.0 - 5.20 \times T$	
${}^0L_{In,Zn:Va} = 33472.0, {}^0L_{In,Sn:Va} = 10460.0, {}^0L_{Sn,Zn:Va} = 12552.0,$	This work
${}^0L_{In,Mg:Va} = -29957.4 - 1.88 \times T, {}^1L_{In,Mg:Va} = -13723.5 - 1.46 \times T, {}^2L_{In,Mg:Va} = -6276.0$	This work
$hcp_{A3}(Zn)$ phase, $(In, Mg, Sn, Zn)(Va)_3$	
$G_{Mg:Va} = {}^0G^{hcp}_{Mg}, G_{Zn:Va} = {}^0G^{hcp\_Zn}_{Zn},$	This work
$G_{In:Va} = {}^*G_{In} + 2000.0, G_{Sn:Va} = {}^*G_{Sn} + 2000.0$	
${}^0L_{Mg,Zn:Va} = -3056.8 + 5.64 \times T, {}^1L_{Mg,Zn:Va} = 3127.3 - 5.66 \times T$	[86]
${}^0L_{Sn,Zn:Va} = 35020.1$	[73]
${}^0L_{In,Zn:Va} = 35020.1, {}^0L_{In,Sn:Va} = 33472.0$	This work
$bct(Sn)$ *phase,* $(In, Mg, Sn, Zn)(Va)_3$	
$G_{Mg:Va} = {}^0G^{hcp}_{Mg} + 15000.0, G_{Zn:Va} = {}^0G^{hcp\_Zn}_{Zn} + 4184.0,$	This work
$G_{In:Va} = {}^*G_{In} + 2092.0, G_{Sn:Va} = {}^*G_{Sn}$	This work
${}^0L_{Sn,Zn:Va} = 5999.9 + 22.50 \times T, {}^0L_{In,Sn:Va} = 460.2$	This work
$tet(In)$ *phase* $(In, Mg, Sn, Zn)(Va)_3$	
$G_{In:Va} = {}^*G_{In}, G_{Sn:Va} = {}^*G_{Sn} + 15000.0, G_{Mg:Va} = {}^0G^{hcp}_{Mg} + 15000.0, G_{Zn:Va} = {}^0G^{hcp}_{Zn} + 17505.9$	This work
${}^0L_{In,Zn:Va} = -12552.0 - 20.08 \times T, {}^0L_{In,Sn:Va} = 836.8 - 1.67 \times T, {}^0L_{Sn,Zn:Va} = 14644.0$	This work
${}^0L_{In,Mg:Va} = -26359.2 + 18.83 \times T$	This work
$MgZn_2$ phase, $(Mg, Zn)_2(Mg, Zn)$	
$G_{Mg:Mg} = 3 \times {}^0G^{hcp}_{Mg} + 23372.7, G_{Mg:Zn} = 2 \times {}^0G^{hcp}_{Mg} + 1 \times {}^0G^{hcp}_{Zn} + 6535.5 - 8.84 \times T, G_{Zn:Zn} = 3 \times {}^0G^{hcp}_{Zn}$ $+15000.0, G_{Zn:Mg} = 2 \times {}^0G^{hcp}_{Zn} + 1 \times {}^0G^{hcp}_{Mg} - 35359.6 + 8.84 \times T$	[86]
$\beta''(L1_0)$ phase, (Mg, In)(Mg, In):	
$G_{Mg:Mg} = {}^0G^{hcp}_{Mg} + 2600.0 + 0.90 \times T, G_{In:In} = {}^*G_{In} + 123.0 - 0.30 \times T,$	This work
$G_{Mg:In} = G_{In:Mg} = {}^*G_{In} + {}^0G^{hcp}_{Mg} - 4479.4 - 0.59 \times T,$	
$L_{Mg,In:Mg} = L_{Mg:Mg,In} = -21756.0 + 0.63 \times T, L_{Mg,In:In} = L_{In:Mg,In} = 627.6 - 0.42 \times T,$	
$\beta', \gamma'(L1_2)$*phase,* $(Mg, In)_3(Mg, In)$	
$G_{Mg:Mg} = 4 \times {}^0G^{hcp}_{Mg} + 10400.0 + 3.6 \times T, G_{In:In} = 4 \times {}^*G_{In} + 492 - 1.20 \times T,$	This work
$G_{Mg:In} = {}^*G_{In} + 3 \times {}^0G^{hcp}_{Mg} + 7923.0 \times +2.4T, G_{In:Mg} = 3 \times {}^*G_{In} + {}^0G^{hcp}_{Mg} - 35540.5 - 1.09 \times T$	
${}^0L_{In:Mg,In} = -32049.4 + 2.93 \times T, {}^1L_{In:Mg,In} = 7949.6,$	
$\beta_1(hR16)$phase, (Mg, In)$_3$(Mg, In):	
$G_{Mg:Mg} = 4 \times {}^0G^{hcp}_{Mg} + 6694.4, G_{In:In} = 4 \times {}^*G_{In},$	This work
$G_{Mg:In} = {}^*G_{In} + 3 \times {}^0G^{hcp}_{Mg} - 35145.6 + 3.18 \times T, G_{In:Mg} = 3 \times {}^*G_{In} + {}^0G^{hcp}_{Mg}$	
$\gamma(InSn)$ *phase,* $(In, Sn)(Va)_3$	
$G_{In:Va} = {}^*G_{In} + 10292.6 - 7.64 \times T, G_{Sn:Va} = {}^*G_{Sn} + 924.7 - 1.76 \times T,$	This work
${}^0L_{In,Sn:Va} = -15480.8 + 18.74 \times T$	
$\beta(InSn)$*phase,* $(In, Sn)(Va)_3$	
$G_{In:Va} = {}^*G_{In}, G_{Sn:Va} = {}^*G_{Sn} + 5015.5 - 7.50 \times T,$	This work
${}^0L_{In,Sn:Va} = 292.0 - 3.14 \times T, {}^1L_{In,Sn:Va} = 627.6 + 0.29 \times T$	
Mg_2Sn phase, $(Mg)_2(Sn) G = -102589.8 + 367.5 \times T - 68.331 \times T \ln T - 0.0178986 \times T^2 + 3.33829 \times 10^{-7} \times T^3 + 95940/T$	[85]
$Mg2Zn3$ phase, $(Mg)_2(Zn)_3$: $G = 2 \times G^{hcp}_{Mg} + 3 \times G^{hcp}_{Zn} - 54406.2 + 13.60 \times T$	[86]
Mg_2Zn_{11} phase, $(Mg)_2(Zn)_{11}$: $G = 2 \times G^{hcp}_{Mg} + 11 \times G^{hcp}_{Zn} - 73818.3 + 18.46 \times T$	[86]
$Mg_{12}Zn_{13}$ phase, $(Mg)_{12}(Zn)_{13}$: $G = 12 \times G^{hcp}_{Mg} + 13 \times G^{hcp}_{Zn} - 236980.8 + 59.23 \times T$	[86]
$Mg_{51}Zn_{20}$phase, $(Mg)_{51}(Zn)_{20}$: $G = 51 \times G^{hcp}_{Mg} + 20 \times G^{hcp}_{Zn} - 335741.5 + 35.40 \times T$	[86]
$InMg_2$ phase, $(In)(Mg)_2$: $G = 2 \times G^{hcp}_{Mg} + {}^*G_{In} - 29022.6 + 1.09 \times T$	This work
In_2Mg_5 phase, $(In)_2(Mg)_5$: $G = 5 \times G^{hcp}_{Mg} + 2 \times {}^*G_{In} - 65022.3 + 5.14 \times T$	This work
${}^*G_{In} = \int {}^*Cp_{In}dt - T \times \int \frac{{}^*Cp_{In}}{T}dt, {}^*G_{Sn} = \int {}^*Cp_{Sn}dt - T \times \int \frac{{}^*Cp_{Sn}}{T}dt$	
${}^*Cp_{Sn} = 25.858 - 0.0010237 \times T - 36,880 \times T^{-2} + 1.9156602 \times 10^{-5} \times T^2$ 249K $< T <$ 250K	
$= 15.961 + 0.0377404 \times T + 123920 \times T^{-2} - 1.8727002 \times 10^{-5} \times T^2$ $251K < T <$ 1000K	
$= 35.098$ 1000K $< T <$ 3000K	
${}^*Cp_{In} = 21.8386 + 0.01145132 \times T + 45,812 \times T^{-2} + 1.2721926 \times 10^{-5} \times T^2 298$ K $< T <$ 429.78K	
$= 31.05 - 0.0001919 \times T - 312000 \times T^{-2} + 3.374 \times 10^{-}8 \times T^2$ 429.79K $< T <$ 3800K	

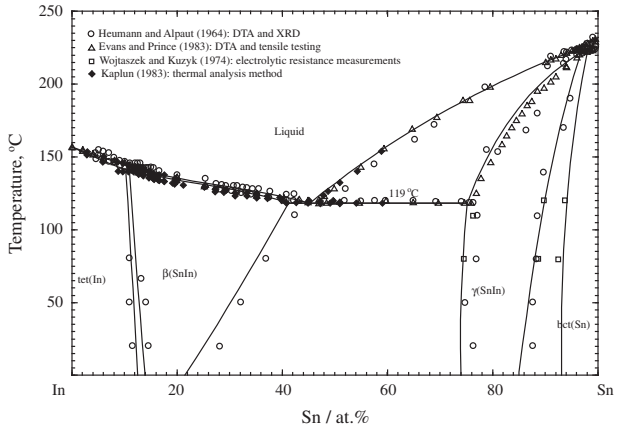

Fig. 7. Calculated In–Sn phase diagram in comparison with the reported experimental data [30–32,34].

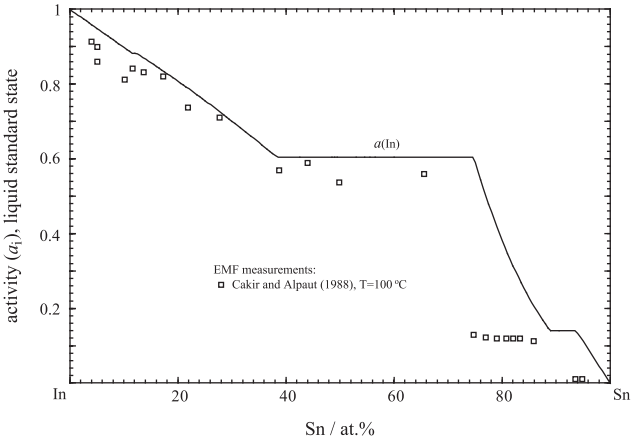

Fig. 10. Calculated activity of In in solid In–Sn binary alloys at 100 °C (reference state tet(In)) in comparison with the reported experimental data [35].

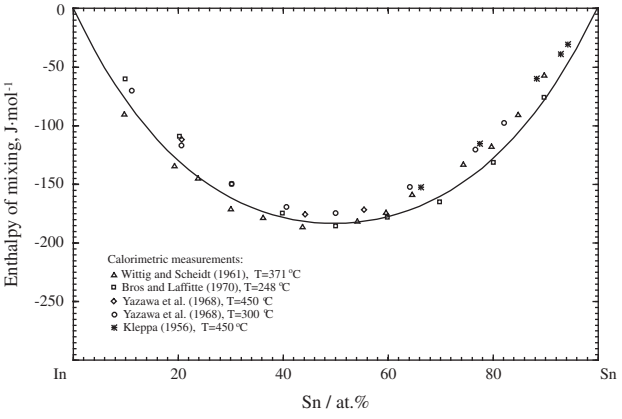

Fig. 8. Calculated enthalpy of mixing of liquid In–Sn binary alloys at 450 °C in comparison with the reported experimental data [40–43].

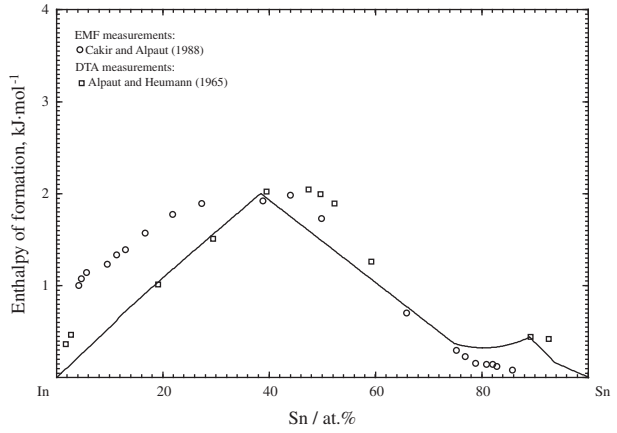

Fig. 11. Calculated enthalpy of formation of solid In–Sn binary alloys at 100 °C in comparison with the reported experimental data [35,45].

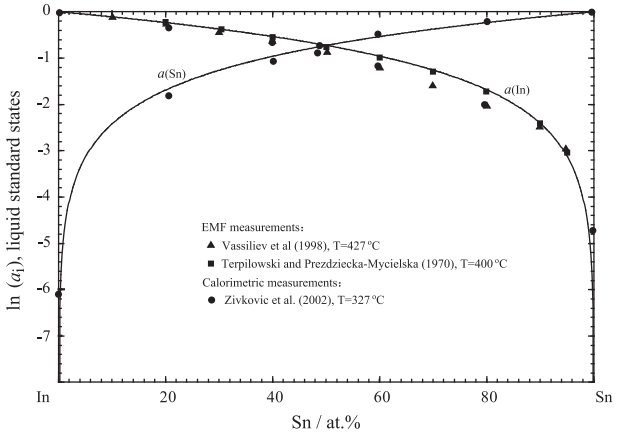

Fig. 9. Calculated activity of In and Sn in the liquid phase at 427 °C in comparison with the reported experimental data [37–39].

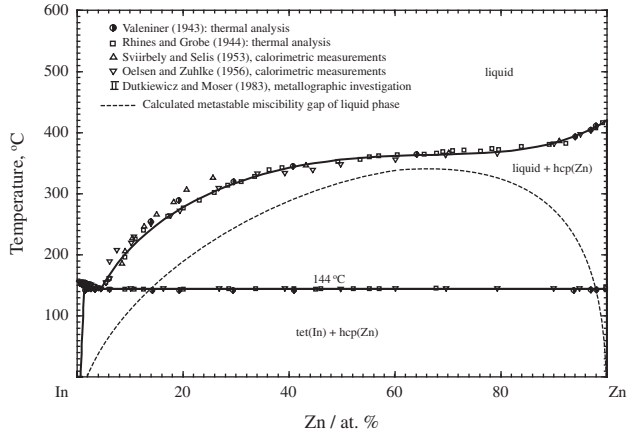

Fig. 12. Calculated In–Zn phase diagram along with the reported experimental data [50–53].

and Zakulski [48]. The phase diagram is constituted of a simple eutectic, *liquid* + *tet*(*In*) ↔ *hcp*(*Zn*), and was first investigated by Wilson and Peretti [49] using the visual polythermal method and optical microscopy. Soon after, Valentiner [50] and Rhines and Grobe [51] modified the phase diagram based on new data obtained by thermal analysis. The phase relations were then determined by Svirbely and Selis [52], Oelsen and Zuhlke [53], Bohl and Hildebrandt [54], and Moser [55] by performing EMF or calorimetric measurements. All the liquidus experimental data are in a good agreement except for the early data collected by Wilson and Peretti [49]. The eutectic temperature was reported to lie in the range of 141.5–144 °C. The temperature of 143.5 °C reported

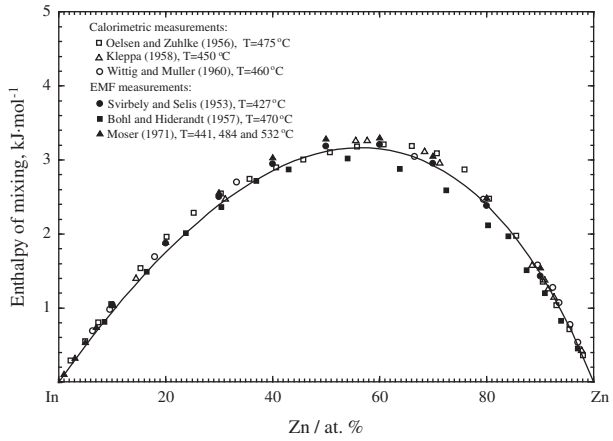

Fig. 13. Calculated enthalpy of mixing of liquid In–Zn binary alloys at 450 °C along with the reported experimental data [52–55,58,59].

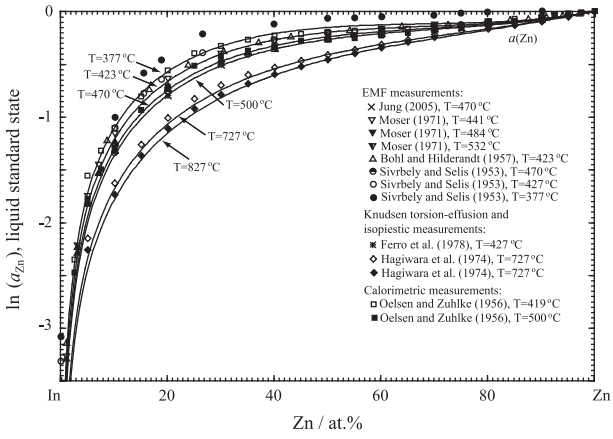

Fig. 14. Calculated activity of Zn in liquid In–Zn binary alloys at temperatures from 423 °C to 857 °C in comparison with the reported experimental data [52–55,60–62].

by Rhines and Grobe [51], which is based on accurate measurements of the cooling curves, was accepted as the most reliable value. Here it should be noted that the overcooling effect on the measurements of eutectic reaction temperature can be ignored in comparison with the effect on liquidus and pretectic temperature measurements. According to the metallographic examinations of Dutkiewicz and Moser [56], In–Zn alloys with 3.1, 3.8 and 4.8 at.% Zn are solidifying with hypoeutectic, eutectic and hypereutectic microstructures, respectively. Considering all the available experimental data, the eutectic composition is located between 3.46 and 3.8 at.% Zn. The maximum solubility of Zn in the tet(In) phase was found to be 2.09 at.% Zn by Rhines and Grobe [51], which is virtually identical to the 2.1 at.% Zn reported later by Nishimura et al. [57]. The solubility of In in the Zn (hcp) terminal solid solution is very limited; less than 0.2 at.% In [57].

The enthalpy of mixing of the liquid phase was investigated by Oelsen and Zuhlke [53], Kleppa [58], and Wittig and Muller [59] using calorimetric measurements, and derived by Svirbely and Selis [52], Bohl and Hildebrandt [54], Moser [55], Jung [60] based on their results from EMF measurements, and by Ferro et al. [61] and Hagiwara et al. [62] based on their results obtained from a Knudsen torsion–effusion and isopiestic measurements respectively. And all their results are in good agreement except the data reported by Bohl and Hildebrandt [54]. The activity of Zn in the liquid phase at different temperatures was studied by several investigators [52,54,55] using EMF measurements, and studied by Ferro et al. [61] and Hagiwara et al. [62] using Knudsen torsion–effusion and isopiestic measurements methods. All the reported thermodynamic experimental data are in a reasonable agreement.

The thermodynamic optimization of In–Zn binary system was carried by Lee et al. [63] with BMW for liquid phase. In order to construct a self-consistent thermodynamic database of Mg–Sn–In–Zn quaternary system, the In–Zn system was re-optimized with the MQMPA for liquid phase in the present work.

2.4. Mg–Sn–In

The phase equilibria in the isothermal section at 300 °C was investigated by Kinzhibalo [64] using XRD. According to him, there is no stable ternary compound in this isothermal section. The activity of Mg in the Mg–Sn–In ternary liquid alloys were studied by Moser and Castanet [65] and by Zakulski et al. [66] using EMF measurements with the cell of the type: $Mg_{(liq.,s)}//(MgCl_2–LiCl–KCl)//Mg–In–Sn_{(liq.,liq.+s)}$.

In order to obtain an accurate and self-consistent thermodynamic optimization of Mg–Sn–In ternary system, the phase

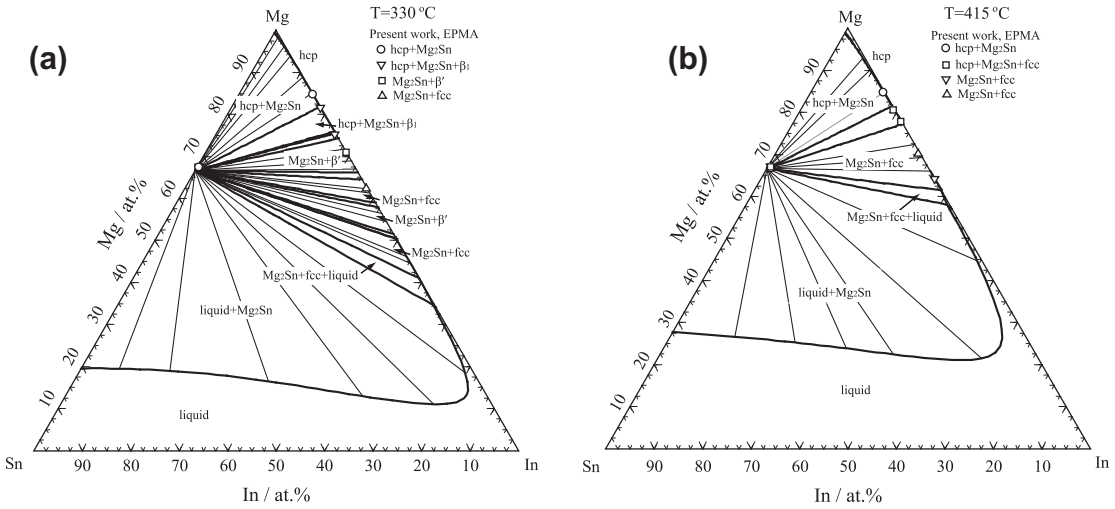

Fig. 15. Calculated isothermal sections of the Mg–Sn–In ternary system at (a) 415 °C and (b) 330 °C along with the present experimental data obtained by EPMA measurements.

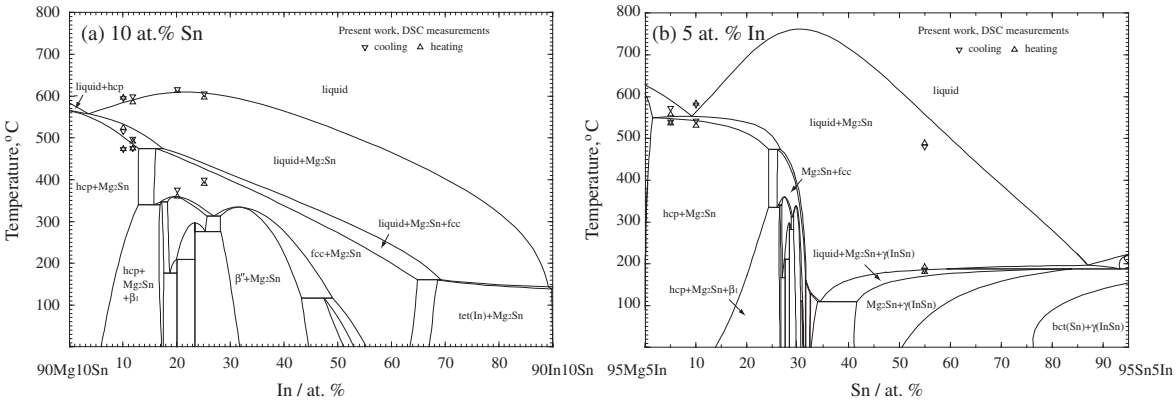

Fig. 16. Calculated ternary isoplethal sections of (a) 10 Sn and (b) 5 In (at.%) in comparison with the present experimental data.

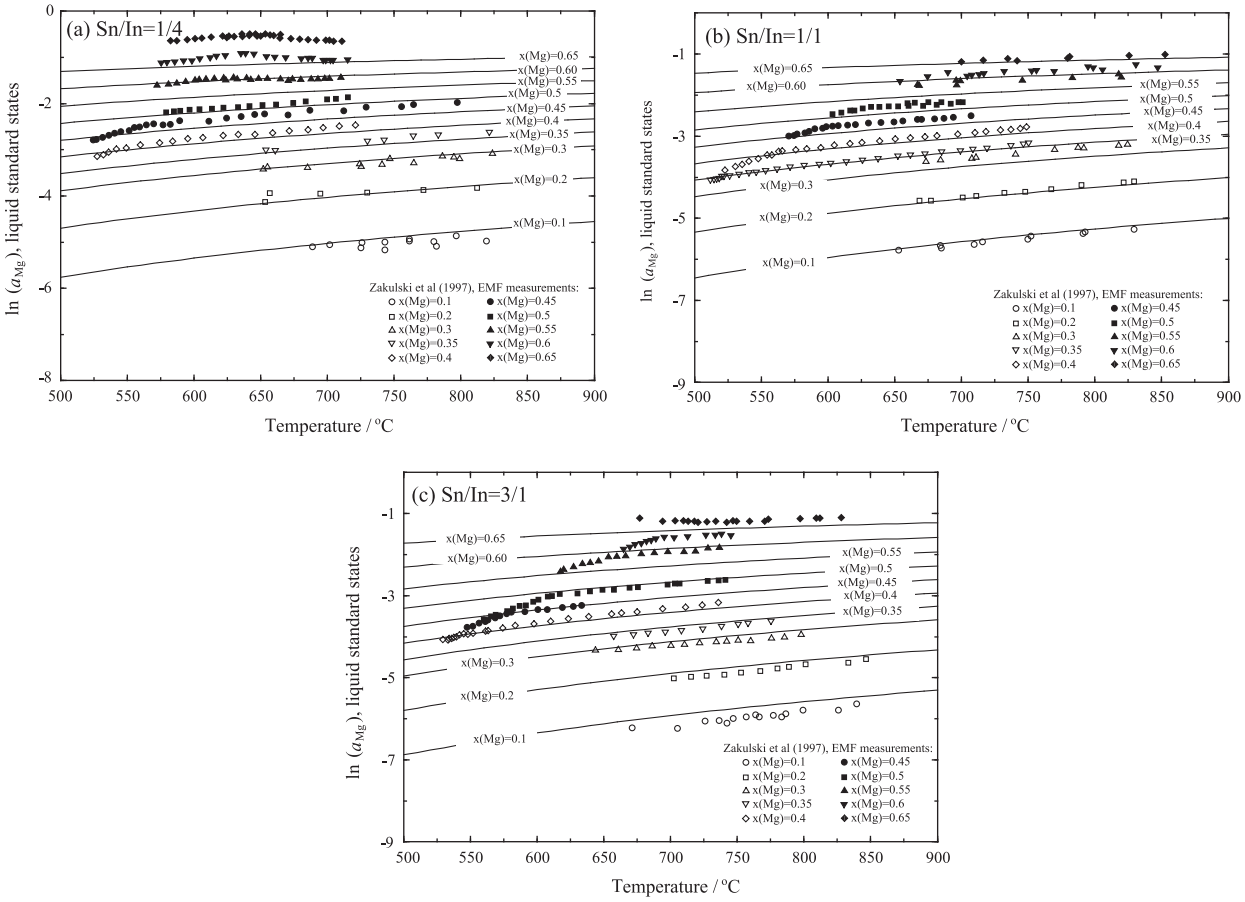

Fig. 17. Calculated activity of Mg (liquid reference states) with the (a) 0.25, (b) 1, (c) 3/1 in liquid Mg–In–Sn ternary alloys versus temperature along with the reported experimental data (corrected for the Mg(s)/Mg(liq.) fusion below 650 °C) [66].

equilibria measurements are needed. Consequently, the isothermal sections at 415 and 330 °C, and isoplethal sections at 10 Sn and 5 In (at.%) were studied in the present work firstly, and then a thermodynamic optimization of Mg–Sn–In ternary was carried out.

2.5. Mg–Sn–Zn

Phase equilibria in the Mg–Sn–Zn ternary system was first studied by Otani [67] using thermal analysis and optical microscopy. Seven ternary isoplethal sections were reported. However, it should be noted that Otani [67] employed an outdated phase diagram for the Mg–Zn system; the currently accepted phase diagram, with five intermediate compounds, was updated by Agarwal et al. [68]. Phase equilibria in the $MgZn_2$–Mg_2Sn–Zn–Sn region were investigated by Godecke and Sommer [69] using thermal analysis and metallographic methods. The liquidus projection and six isoplethal sections were determined. According to Otani [67] and Godecke and Sommer [69], no stable ternary compound exists in the Mg–Sn–Zn system. The ternary solubility of Sn in Mg–Zn binary compounds and of Zn in Mg_2Sn was studied by Mingolo et al. [70] and Sirkin et al. [71] using Mossbauer spectroscopy and XRD. According to them, there is a limited solid solubility

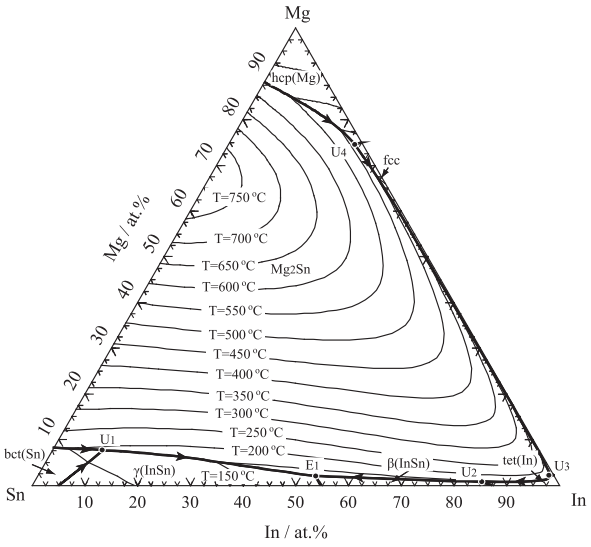

Fig. 18. Calculated liquidus projection of the Mg-Sn-In ternary system.

Table 7
Calculated invariant reactions in the liquidus projection of the Mg–Sn–In ternary system.

Label	Temperature (°C)	Reaction	Composition of liquid (at.%)		
			Mg	In	Sn
E1	110	$L \leftrightarrow \gamma(InSn) + \beta(InSn) + Mg_2Sn$	2.02	52.69	45.30
U1	188	$L + bct(Sn) \leftrightarrow \gamma(InSn) + Mg_2Sn$	7.65	9.52	82.82
U2	136	$L + tet(In) \leftrightarrow \beta(InSn) + Mg_2Sn$	0.81	84.34	14.85
U3	160	$L + fcc \leftrightarrow tet(In) + Mg_2Sn$	2.28	97.13	0.59
U4	474	$L + hcp \leftrightarrow fcc + Mg_2Sn$	74.62	23.88	1.50

of Sn in Mg–Zn binary compounds and of Zn in Mg_2Sn. For Gladyshevsky and Cherkashin [72], the ternary solubility of Sn in $MgZn_2$ reaches 3.6 wt.% at 400 °C. Later, Godecke and Sommer [69] measured a maximum solubility of about 0.7 wt.% by using thermal analysis and optical microscopy, which is in a reasonable agreement with Gladyshevsky and Cherkashin [72] and our own results considering experimental errors.

Although, many experimental results of the phase equilibria measurements were reported in previously [67–72], the phase equilibra information of isothermal sections is still lacking. Furthermore, the data of solid solubility for Sn in Mg–Zn binary compound is also limited, which is important for studying the solidification behavior of the Mg based alloys. Consequently, the ternary isothermal section of Mg–Zn–Sn at 330 °C was firstly studied in the present work.

A thermodynamic assessment of the Mg–Zn–Sn ternary system was obtained by Ghosh et al. [73] and by Meng et al. [74], and their optimization results are in a reasonable agreement with all the reported data. In order to obtain an accurate and self-consistent thermodynamic optimization of Mg–Sn–In–Zn ternary system, the thermodynamic optimization was carried out in the present work with the MQMPA for liquid solution, taking into account the current experimental data and those reported in the literature [67–72].

2.6. In–Sn–Zn system

The liquidus projection and numerous isoplethal sections of the In–Sn–Zn system were determined by Yoon et al. [75] using DSC, scanning electron microscopy (SEM) and XRD. Xie et al. [76] measured the isoplethal sections at Sn/Zn molar ratios of 2:1, 1:1 and 1:2 and ternary isoplethal section at constant 10 at.% In by using DTA, XRD and EPMA. Recently, Sabbar et al. [77] determined with DSC six isoplethal sections with In/Sn molar ratios of 5:95, 15:85, 1:2, 52:48, 2:1 and 85:15.

Moser [78] reported the activity of Zn in In–Sn liquid solutions with 3 wt.% Zn by using EMF measurements at 441 °C, 484 °C and 532 °C. Fiorani et al. [79] studied the enthalpy of mixing of the In–Sn–Zn liquid phase by using a Calvet-type drop calorimeter. Nakamura et al. [80] studied the thermodynamic properties of the In–Sn–Zn liquid phase with the In/Sn molar ratios of 1:1, 3:1 and 1:3 by using EMF measurements. Later, Anres et al. [81] measured the enthalpy of mixing of the In–Sn–Zn liquid phase with the In/Sn molar ratios of 1:3, 1:1, 3:1, and Zn/In molar ratios of 1:3 and 1:1 at 440 °C and 634 °C by using a direct-reaction calorimeter. Recently, Rechchach et al. [44] reported the enthalpy of mixing of the In–Sn–Zn liquid phase with the In/Sn ratios of 1.795, 0.506, 0.999, 2.01, and 5.702 at 500 °C by using a direct-reaction calorimeter. A thermodynamic modeling of the In–Sn–Zn ternary system was obtained by Xie et al. [82] and by Cui et al. [83] both using a BWM for liquid phase. In order to get a self-consistent and more critical evaluated thermodynamic database for the Mg–Sn–In–Zn quaternary system, the In–Sn–Zn ternary system was critical evaluated and re-optimized using MQMPA for the liquid phase.

3. Thermodynamic modeling

In the present work, the thermodynamic optimization of the Mg–Sn–In–Zn quaternary system was carried out by means of the FactSage thermodynamic software [84]. All phases considered

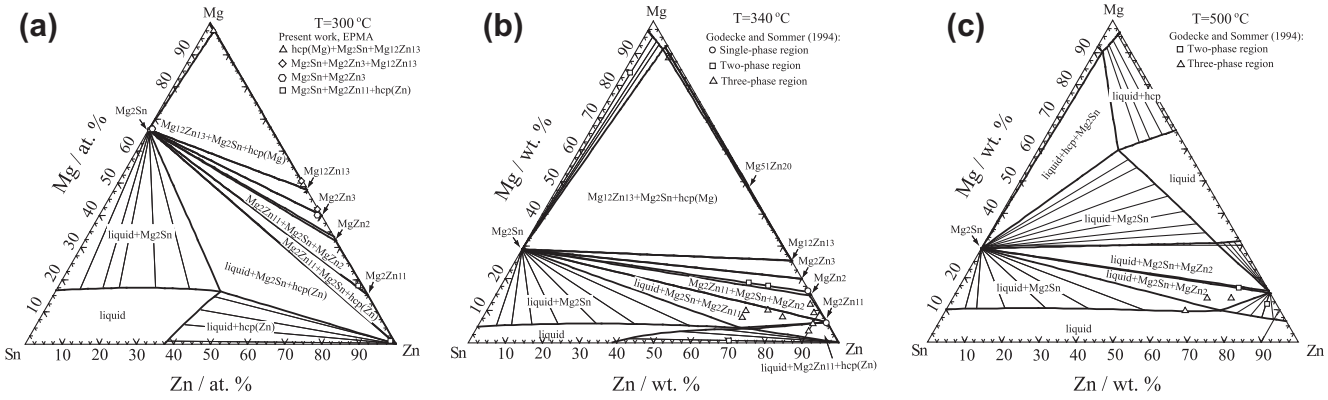

Fig. 19. Calculated isothermal sections of the Mg–Sn–Zn ternary system at (a) 300 °C, (b) 340 °C and (c) 500 °C compared with present and reported experimental data [69].

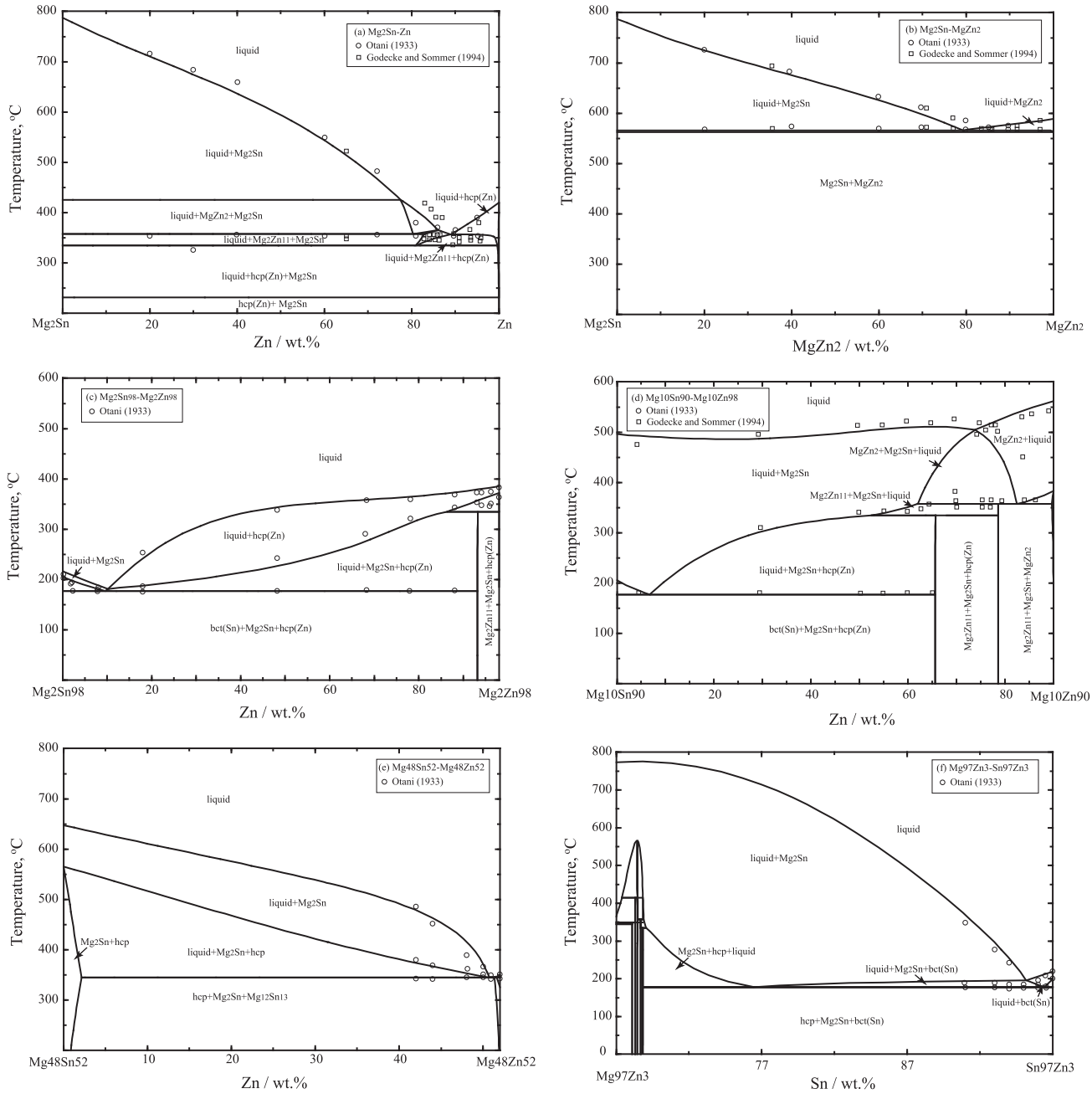

Fig. 20. Calculated isoplethal sections of the Mg–Sn–Zn ternary system (a) Mg_2Sn–Zn, (b) Mg_2Sn–$MgZn_2$, (c) Mg2Sn98–Mg2Zn98, (d) Mg10Sn90–Mg10Zn90, (e) Mg48Sn52–Mg48–Zn52, (f) Mg97Zn3–Sn97Zn3, (g) Mg30Zn70–Mg30Sn70, (h) Mg10Zn90–Sn10Zn90, (i) Mg98Sn2–Zn98Sn2, (j) Mg90Sn10–Zn90Sn10, (k) Mg60Sn40–Zn60Sn40, and (l) Mg15Sn85–Zn15Sn85 along with the reported experimental data [67,69].

in the Mg–Sn–In–Zn quaternary system are listed in Table 1, along with the model used to describe their thermodynamic properties. The binary systems Mg–Sn, Mg–Zn and Sn–Zn have been critical evaluated and parameters of their thermodynamic models have been optimized by Jung et al. [85], Spencer [86] and Ghosh et al. [73] using MQMPA for the liquid solution. Consequently, all the thermodynamic parameters of Mg–Sn, Mg–Zn and Sn–Zn binary systems were taken from their work [73,85,86] without further modification for the present optimization of the Mg–Sn–In–Zn quaternary system.

3.1. Liquid phase

The thermodynamic properties of the liquid phase were modeled using the Modified MQMPA developed by Pelton et al. [46,47]. A detailed description of the MQMPA and its associated notation is given in Refs. [46,47]. The same notation is used in the present work, and a brief description of MQMPA is given as follows:

For the binary $(A + B)$ system, the quasichemical pair exchange reaction can be considered:

$$(A{-}A)_{pair} + (B{-}B)_{pair} = 2(A{-}B)_{pair},\ \Delta g_{AB} \tag{1}$$

where $i - j$ pair represents a first-nearest-neighbor pair of atoms. The Gibbs energy change for the formation of one mole of $(A–B)$ pairs according to Reaction (1) is $\Delta g_{AB}/2$. Let n_A and n_B be the number of moles of A and B, n_{AA}, n_{BB}, and n_{AB} be the number of moles of A–A, B–B and A–B pairs. Z_A and Z_B are the coordination numbers of A and B. Then the Gibbs energy of the solution is given by:

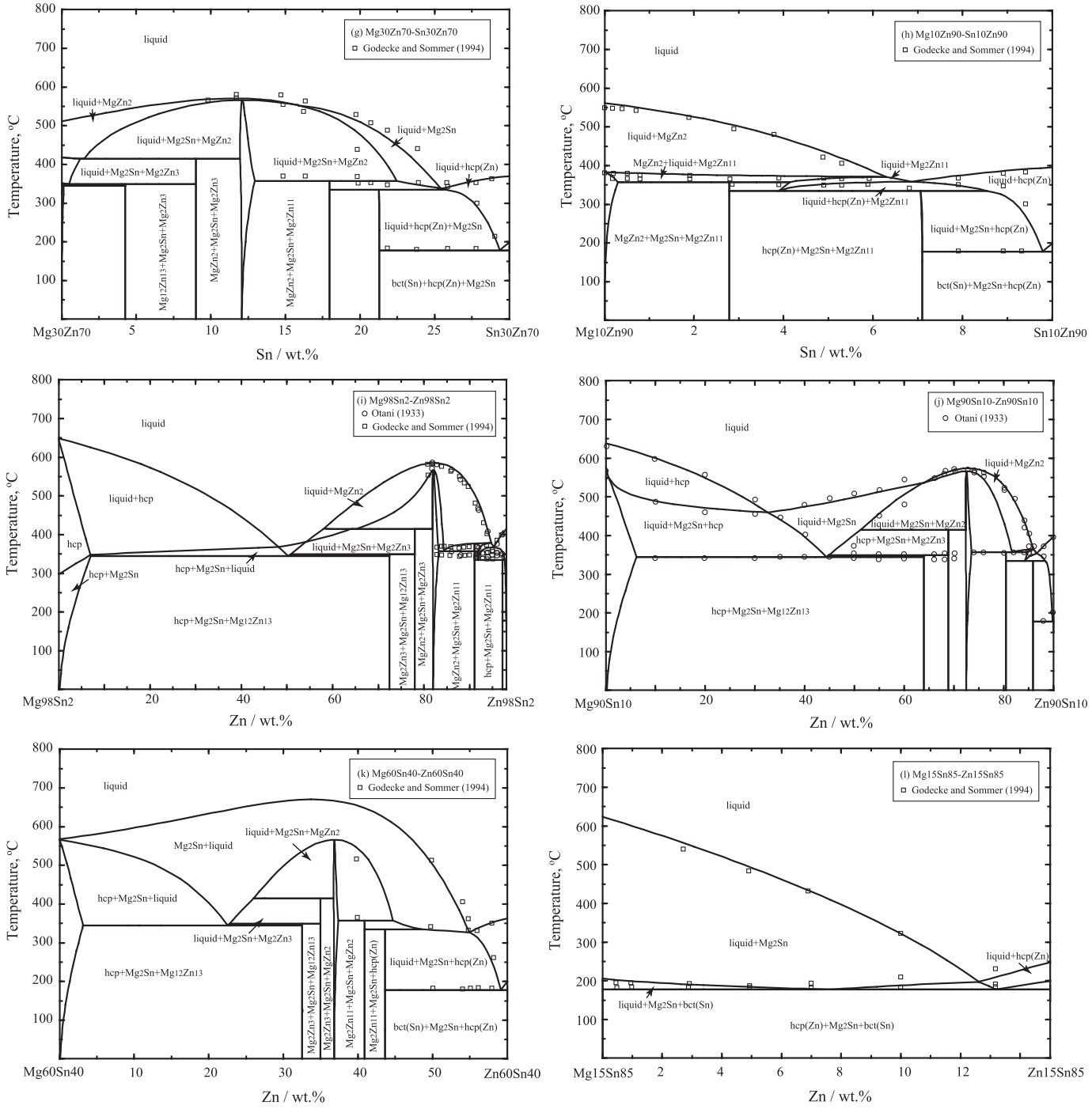

Fig. 20 (*continued*)

$$G = \left(n_A G_A^o + n_B G_B^o\right) - T\Delta S^{config} + (n_{AB}/2)\Delta g_{AB} \quad (2)$$

where G_A^o and G_B^o are the molar Gibbs energies of the pure component A and B, and ΔS^{config} is the configurational entropy of mixing given by randomly distributing the A–A, B–B and A–B pairs in the one-dimensional Ising approximation. The expression for ΔS^{config} is:

$$\Delta S^{config} = -R(n_A \ln X_A + n_B \ln X_B) - R\left(n_{AA} \ln \frac{X_{AA}}{Y_A^2} + n_{BB} \ln \frac{X_{BB}}{Y_B^2} + n_{AB} \ln \frac{X_{AB}}{2Y_A Y_B}\right) \quad (3)$$

where X_{AA}, X_{AB} and X_{BB} are the mole fractions of the A–A, B–B and A–B pairs respectively; Y_A and Y_B are the coordination-equivalent fractions of A and B:

$$X_{ij} = \frac{n_{ij}}{n_{AA} + n_{BB} + n_{AB}} (i,j = A \text{ or } B) \quad (4)$$

$$Y_i = \frac{Z_i n_i}{Z_A n_A + Z_B n_B} \quad (i = A \text{ or } B) \quad (5)$$

Moreover, the following elemental balance equations can be written:

$$Z_A n_A = 2n_{AA} + n_{AB} \quad (6)$$

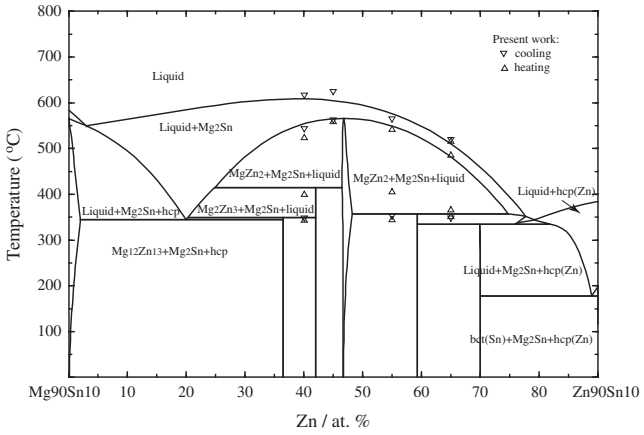

Fig. 21. Calculated isoplethal section at 10 at.% Sn in the Mg–Sn–Zn system along with the experimental data obtain in the present work from DSC measurements.

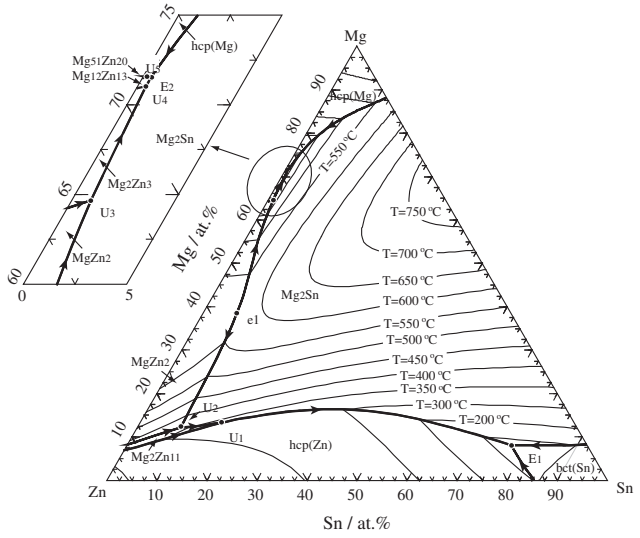

Fig. 22. Calculated liquidus projection of the Mg–Sn–Zn ternary system.

Table 8
Calculated invariant reactions in the liquidus projection of the Mg–Sn–Zn ternary system.

Label	Temperature (°C)	Reaction	Composition of liquid (at.%)		
			Mg	Zn	Sn
e1	566	$L \leftrightarrow MgZn_2 + Mg_2Sn$	38.98	54.63	6.39
E1	177	$L \leftrightarrow bct(Sn) + hcp\ Zn + Mg_2Sn$	8.07	15.12	76.81
U1	335	$L + Mg_2Zn_{11} \leftrightarrow hcp\ Zn + Mg_2Sn$	13.30	40.32	16.38
U2	357	$L + MgZn_2 \leftrightarrow Mg_2Zn_{11} + Mg_2Sn$	12.19	79.20	8.61
U3	414	$L + MgZn_2 \leftrightarrow Mg_2Zn_3 + Mg_2Sn$	64.66	34.41	0.93
U4	349	$L + Mg_2Zn_3 \leftrightarrow Mg_{12}Zn_{13} + Mg_2Sn$	70.03	28.56	4.18
U5	345	$L + Mg_{51}Zn_{20} \leftrightarrow Mg_{12}Zn_{13} + hcp$	71.54	28.25	2.08
E2	344.6	$L \leftrightarrow Mg_{12}Zn_{13} + Mg_2Sn + hcp$	71.53	28.08	3.94

$$Z_B n_B = 2n_{BB} + n_{AB} \tag{7}$$

It may be noted that there is no exact expression for the configurational entropy in three dimensions. Although Eq. (3) is only an approximate expression in three dimensions, it is exact one-dimensionally (when $Z = 2$) [47]. As explained in [47], one is forced by the approximate nature of Eq. (3) to use non-exact values for the coordination numbers in order to yield good fits between the experimental data and calculated ones. The mathematical approximation of the one-dimensional Ising model of Eq. (3) can be partially compensated by selecting values of Z_A and Z_B which are smaller than the experimental values [87]. As is known, the MQMPA model is sensitive to the ratio of coordination numbers, but less sensitive to their absolute values. From a practical standpoint for the development of large thermodynamic databases, values of Z_A and Z_B of the order of 6 have been found necessary for the solutions with a small or medium degree of ordering (*i.e.* alloy solutions).

Δg_{AB} is the model parameter to reproduce the Gibbs energy of liquid phase of the *A–B* binary system, which is expanded as a polynomial in terms of the pair fractions, as follows:

$$\Delta g_{AB} = \Delta g^{o}_{AB} + \sum_{i\geqslant 1} g^{io}_{AB}(X_{AA})^{i} + \sum_{j\geqslant 1} g^{oj}_{AB}(X_{BB})^{j} \tag{8}$$

where Δg^{o}_{AA} g^{io}_{AB} and g^{oj}_{AB} are the adjustable model parameters which can be function of the temperature. The equilibrium state of the system is obtained by minimizing the total Gibbs energy at constant elemental composition, temperature and pressure. The equilibrium pair distribution is calculated by setting:

$$\left(\frac{\partial G}{\partial n_{AB}}\right)_{n_A, n_B} = 0 \tag{9}$$

This gives the "equilibrium constant" for the "quasichemical pair reaction" of Eq. (1):

$$\frac{X^2_{AB}}{X_{AA}X_{BB}} = 4 \times exp\left(-\frac{\Delta g_{AB}}{RT}\right) \tag{10}$$

Moreover, the model permits Z_A and Z_B to vary with composition as follows [47]:

$$\frac{1}{Z_A} = \frac{1}{Z^A_{AA}}\left(\frac{2n_{AA}}{2n_{AA}+n_{AB}}\right) + \frac{1}{Z^A_{AB}}\left(\frac{n_{AB}}{2n_{AA}+n_{AB}}\right) \tag{11}$$

$$\frac{1}{Z_B} = \frac{1}{Z^B_{BB}}\left(\frac{2n_{BB}}{2n_{BB}+n_{AB}}\right) + \frac{1}{Z^B_{AB}}\left(\frac{n_{AB}}{2n_{BB}+n_{AB}}\right) \tag{12}$$

where Z^A_{AA} and Z^A_{AB} are the values of Z_A when all nearest neighbors of an atom *A* are *A*s, and when all nearest neighbors of an atom *A* are *B*s respectively. Z^B_{BB} and Z^B_{AB} are defined similarly. The composition of maximum short-range ordering (SRO) is determined by the ratio of the coordination numbers Z^A_{AB}/Z^B_{AB}. The values of the coordination numbers chosen in the present study are listed in Table 2.

The Gibbs energy of the liquid solution in a ternary system can be interpolated from the Gibbs energies of the three sub-binary systems with different interpolation techniques based on the nature of this ternary system, and small external model parameters will be introduced into the models to get more self-consistent results with the experimental data if they are necessary. The Gibbs energy of all ternary liquid phases are calculated using a symmetric "Kohler-like" [88] type of ternary interpolation technique.

3.2. Solid solutions

The Compound Energy Formalism (CEF) was introduced by Hillert [89] to describe the Gibbs energy of solid phases with sub-lattices. Ideal mixing of species on each sub-lattice is assumed. In the present work, all the solid solutions (hcp, bct, tet and Zn (hcp)) and the ordered intermetallic solutions in the Mg–Sn–In–Zn quaternary system were modeled with the CEF based on their crystal structure. The Gibbs energy expressions are based on the each sub-lattice model, and the details were descript in the Hillert's work [89].

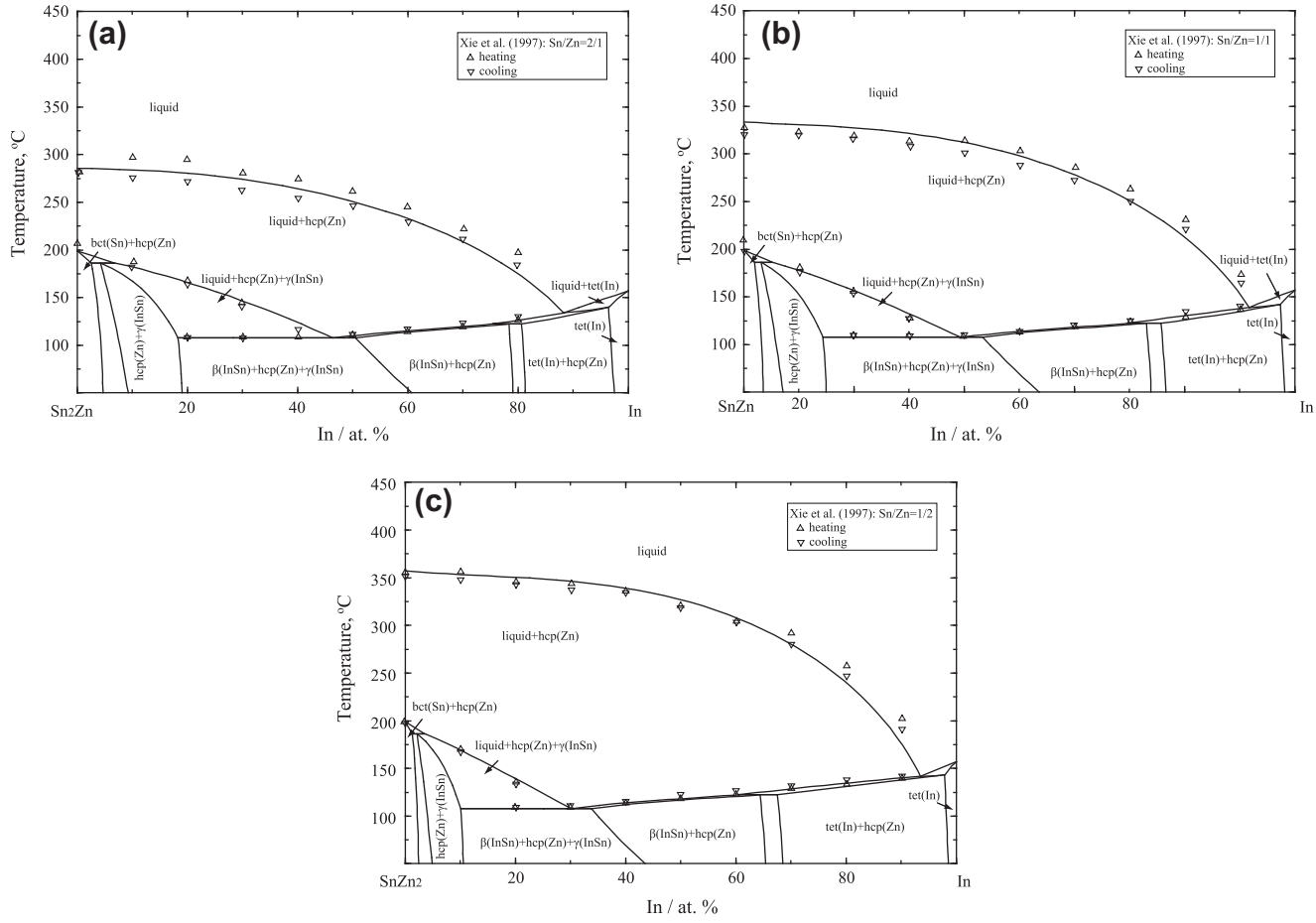

Fig. 23. Calculated isoplethal sections of the In–Sn–Zn ternary system for Sn/Zn molar ratios of (a) 2:1, (b) 1:1 and (c) 1:2 in comparison with the reported experimental data [76].

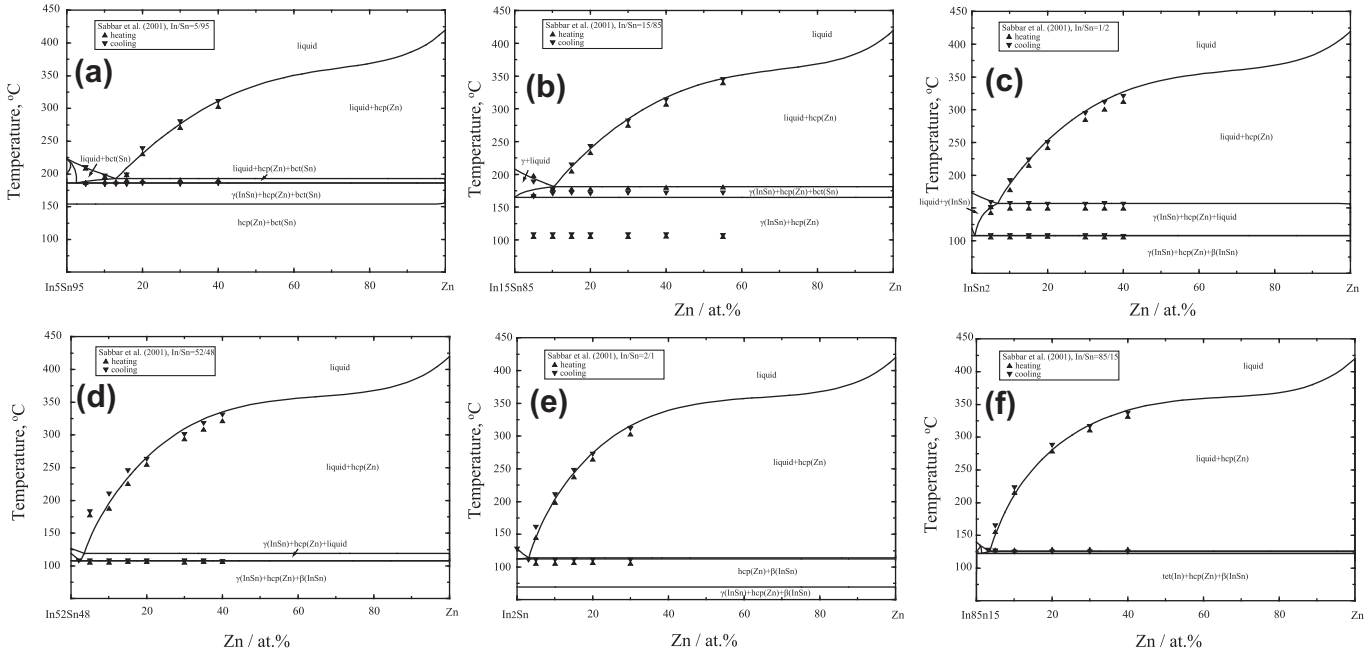

Fig. 24. Calculated isoplethal sections of the In–Sn–Zn ternary system for In/Sn molar ratios of (a) 5:95, (b) 15:85, (c) 1:2, (d) 52:48, (e) 2:1, and (f) 85:15 in comparison with the reported experimental data [77].

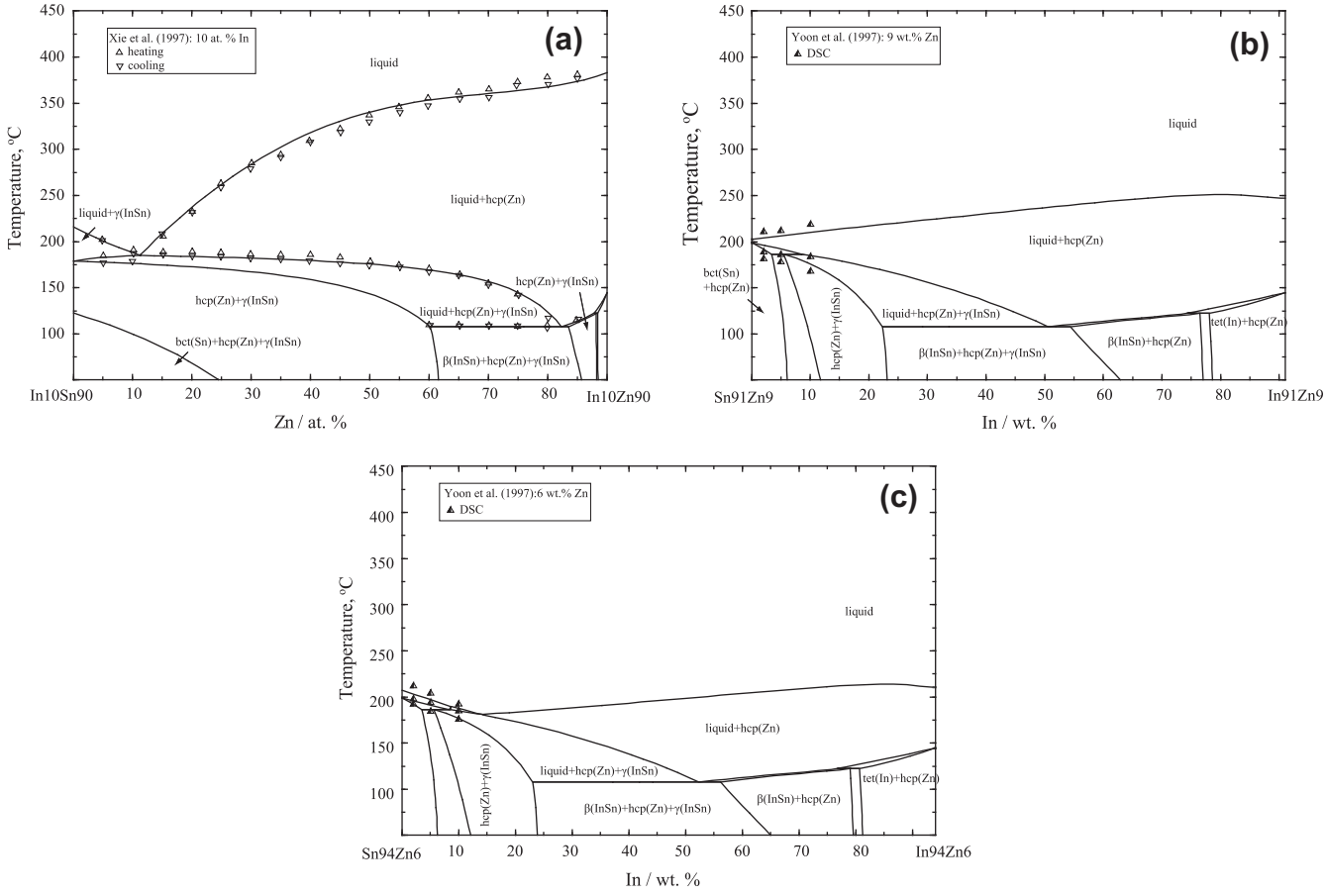

Fig. 25. Calculated isoplethal sections of the In–Sn–Zn system at constant (a) 10 In (at.%), (b) 9 Zn (wt.%), (c) 6 Zn (wt.%) in comparison with the reported experimental data [76,92].

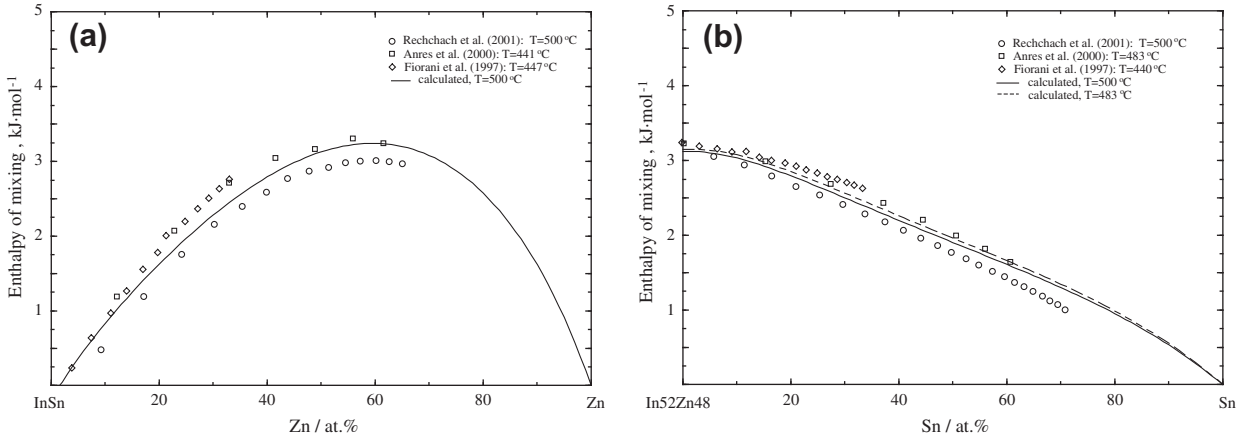

Fig. 26. Calculated mixing enthalpies of ternary liquid In–Sn–Zn alloys (a) with the In/Sn molar ratio of 1:1, and (b) the In/Zn molar ratio of 52:48 and 1:1 at various temperatures along with the reported experimental data [44,79,81].

3.3. Stoichiometric phases

The molar Gibbs energies of pure elements and stoichiometric phases can be described by:

$$G_T^o = H_T^o - TS_T^o \tag{13}$$

$$H_T^o = \Delta H_{298.15K}^o + \int_{T=298.15K}^{T} C_p\,dT \tag{14}$$

$$S_T^o = S_{298.15K}^o + \int_{T=298.15K}^{T} (Cp/T)dT \tag{15}$$

where $\Delta H_{298.15K}^o$ is the molar enthalpy of formation of a given species from pure elements ($\Delta H_{298.15K}^o$ of element stable at 298.15 K and 1 atm is assumed as 0 J mol^{-1}; reference state), $S_{298.15K}^o$ is the absolute third law molar entropy at 298.15 K and C_p is the molar heat capacity.

In the present study, the Gibbs energy of pure elements were taken from the SGTE database [90]. As there are no experimental

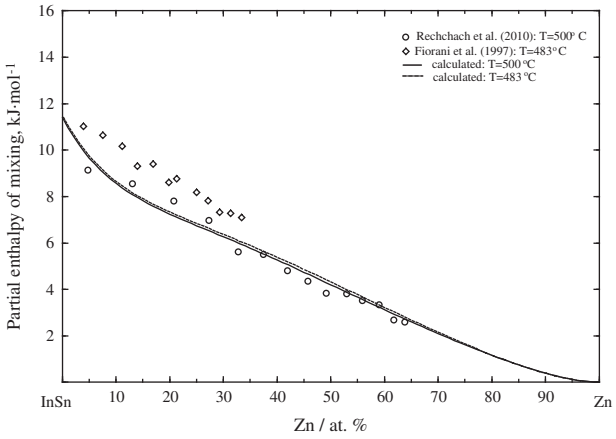

Fig. 27. Calculated partial molar enthalpy of mixing of Zn in liquid In–Sn–Zn alloys at 500 °C compared with the reported experimental data [44].

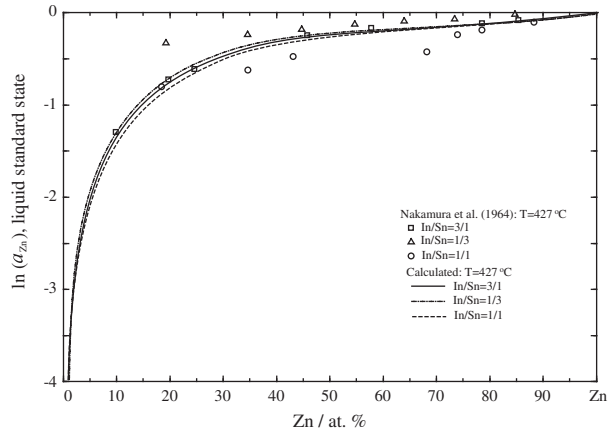

Fig. 28. Calculated activity of Zn in the In–Sn–Zn liquid phase with the In/Sn molar ratios of 1:3, 1:1 and 3:1 along with the reported experimental data [80].

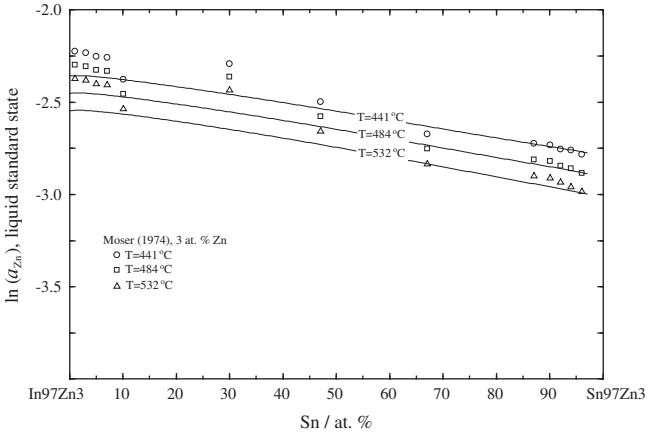

Fig. 29. Calculated activity of Zn in the In–Sn–Zn liquid phase at constant 3 Zn (at.%) in comparison with the reported experimental data [78].

heat capacity data for Ag–In, Ag–Sn and Ag–Mg intermetallics, their heat capacities were evaluated using the Neumann–Kopp rule [91]. The heat capacity of solid In and Sn from the SGTE database show a maximum just above their melting points (that is in the liquid stable region). Consequently, the heat capacity of several

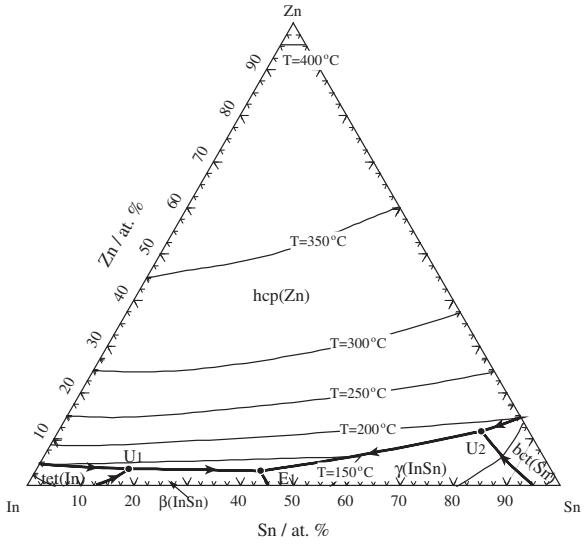

Fig. 30. Calculated liquidus projection of the In–Sn–Zn ternary system.

Table 9
Calculated invariant reactions in the liquidus projection of the In–Sn–Zn ternary system.

Label	Temperature (°C)	Reaction	Composition of liquid (at.%)		
			In	Zn	Sn
E1	107	$L \leftrightarrow \beta(InSn) + \gamma(InSn) + hcp(Zn)$	54.78	3.07	42.16
U1	121	$L + tet(In) \leftrightarrow \beta(InSn) + hcp(Zn)$	79.10	3.52	17.38
U2	186	$L + bct(Sn) \leftrightarrow \gamma(InSn) + hcp(Zn)$	8.88	11.68	79.44

intermetallic phases in the studied system obtained with Neumann–Kopp rule had also a maximum at about 506 K, which is not likely. In order to resolve this, the heat capacity of solid In and Sn above their melting points were adjusted in the present work, which makes it possible for the heat capacity of intermetallics to increase with temperature until the melting point. This was solely applied when the Neumann–Kopp rule was employed and does not influence pure In and Sn.

4. Experimental procedures

Mg–Sn–In and Mg–Sn–Zn ternary alloys were prepared with pure Mg (99.8 wt.%), Sn (99.9 wt.%), In (99.99 wt.%) and Zn (99.5 wt.%) from Alfa Aesar and melted in a frequency induction furnace under argon atmosphere. In order to minimize the interaction of sample with the crucibles, cubic-shaped crucibles with Ta foil (99.5 wt.% purity, 0.15 mm thickness) were prepared. Each alloy was remelted three times in the crucible in order to obtain a homogeneous alloy; the loss due to evaporation was less than 5 wt.% for each sample. Mg–Sn–In samples were sealed into quartz capsules under argon atmosphere and equilibrated at 415 °C for 20 days and at 330 °C for 35 days, respectively. The Mg–Sn–Zn samples were sealed into quartz capsules under argon atmosphere, and equilibrated at 330 °C for 50 days. These temperatures were chosen because they correspond to the temperatures at which heat treatment is usually performed on Mg alloys. Quenching was carried out in water without breaking the quartz tubes.

Electron probe microanalysis (EPMA) of the quenched samples was performed with the JEOL 8900 probe at McGill University using wavelength-dispersive spectrometry (WDS). An accelerating voltage of 15 kV was used with a 20 nA beam current, a spot size of 2 μm and counting times of 20 s on peaks and 10 s on backgrounds. Raw data were reduced with the PRZ correction using pure Mg, Sn, In and Zn metal standards.

The constituent phases of the quenched samples were identified by X-ray diffraction (XRD). XRD patterns were obtained with the PANanalytical Xpert Pro powder X-ray diffractometer at Concordia University using Cu Kα radiation at 45 kV and 40 mA. The spectra were acquired from 20 to 120° 2θ with a 0.02° step size. The collected patterns were analyzed with the X'Pert HighScore Plus analysis software using the Pearson's crystal database.

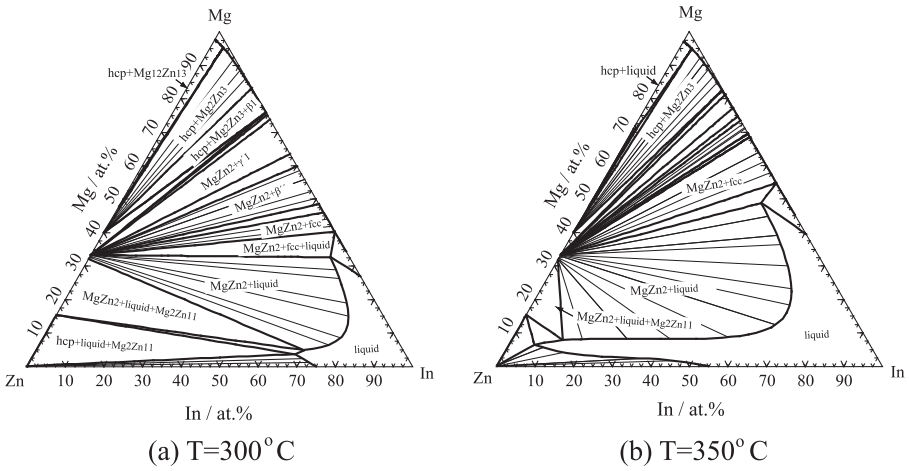

Fig. 31. Calculated isothermal sections at (a) 300 °C, and at (b) 350 °C of the Mg–In–Zn ternary system.

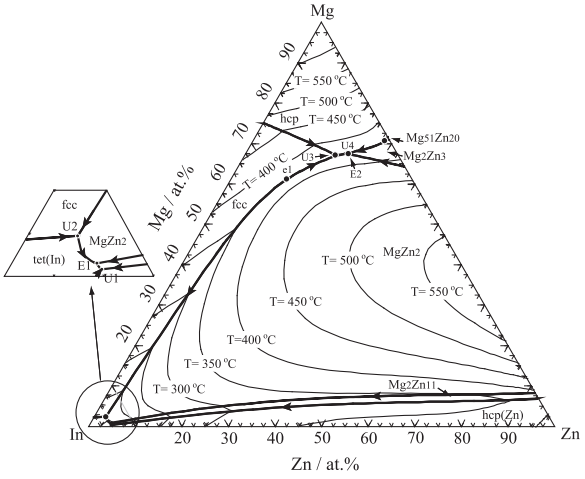

Fig. 32. Calculated liquidus projection of the Mg–In–Zn ternary system.

Liquidus and polymorphic transformation temperatures were measured by differential scanning calorimetry (DSC) using the SETARAM instrumentation at Concordia University. Experiments were carried out by using sintered Al_2O_3 crucibles under flowing argon gas with heating and cooling rates of 5 °C/min. No reaction was observed between the samples and the sintered Al_2O_3 crucibles.

5. Experiment and optimization results

5.1. Experimental results

5.1.1. The Mg–Sn–In system

BSE (back-scattered electron) images of typical ternary Mg–Sn–In alloys are shown in Fig. 1a and b. Phase identification was based on the EPMA and XRD results. In the Mg78Sn10In12 (at.%) alloy quenched from 415 °C, the three-phase equilibrium microstructure hcp(Mg)–Mg_2Sn–fcc was observed (Fig. 1a). Isothermal sections of the Mg–Sn–In ternary system in the Mg-rich region at 415 °C and 330 °C were measured and no ternary compound was found in. All the phase equilibrium compositions determined in the present work are listed in Table 3. The solid solubility of In in Mg_2Sn is less than 0.4 at.%, and the solid solubility of Sn in the fcc and β_1 Mg–In binary compounds is 0.15 and 0.38 at.%, respectively. Since these values are within the error limits of the EPMA measurements, the solubilities are considered negligible. The isoplethal sections in the Mg–In–Sn system at constant 10 Sn and 5 In (at.%) were measured by the DSC technique. The DSC curve of Mg78Sn10In12 alloy is shown in Fig. 2a. Three exothermic peaks were observed in the cooling spectrum, which were well repeated during heating with two endothermic peaks and one weak liquid peak. All the thermal singles obtained from the DSC measurements are presented in Table 4.

5.1.2. The Mg–Sn–Zn system

We experimentally determined the isothermal section at 300 °C of the Mg–Sn–Zn ternary system. No ternary compound was found. BSE (Back-scattered electron) images of typical ternary Mg–Sn–Zn alloys are shown in Fig. 1c and d. In the key sample of Mg25Sn10Zn65 (at.%) quenched from 300 °C, a three-phase equilibrium microstructure Mg_2Zn_{11} + Mg_2Sn + hcp (Zn) was observed (Fig. 1c). And three-phase equilibrium microstructure of Mg_2Sn + $Mg_{12}Zn_{13}$ + hcp (Mg) was observed in the key sample of Mg70Sn10Zn20 as shown in Fig. 1d. The ternary isoplethal with constant 10 Sn (at.%) was determined in the present work with DSC technique, The DSC curve of Mg25Sn10Zn65 alloy is shown in Fig. 2b, two exothermic peaks were observed in the cooling spectrum, one strong endothermic peak and three weak peaks were observed in the heating spectrum. The final liquid peaks are

Table 10
Calculated invariant reactions in the liquidus projection of the Mg–Zn–In ternary system.

Label	Temperature (°C)	Reaction	Composition of liquid (at.%)		
			Mg	Zn	In
e1	377	$L \leftrightarrow fcc + MgZn_2$	61.90	12.46	25.64
E1	147	$L \leftrightarrow tet(In) + MgZn_2 + Mg_2Zn_{11}$	0.45	4.25	95.00
E2	366.3	$L \leftrightarrow hcp + MgZn_2 + Mg_2Zn_3$	67.46	21.24	11.30
U1	145	$L + hcp(Zn) \leftrightarrow Mg_2Zn_{11} + MgZn_2 + tet(In)$	0.41	4.68	94.91
U2	153	$L + fcc \leftrightarrow tet(In) + MgZn_2$	2.35	2.53	95.12
U3	366.4	$L + fcc \leftrightarrow hcp + MgZn_2$	67.07	19.61	13.32
U4	349	$L + Mg_{51}Zn_{20} \leftrightarrow hcp + Mg_2Zn_3$	71.05	28.42	0.53

well repeated during heating and cooling occurring at 518 °C and 521 °C. The endothermic peak occurring at 485 °C should be overlapped in the cooling spectrum because it is close to the first exothermic reaction occurring at 521 °C. All the thermal signals obtained from the DSC measurements are presented in Table 4. All the phase equilibria compositions determined in the present work are listed in Table 3. As for the Mg–Sn–In ternary system, there is limited solubility of Zn in the Mg_2Sn compound (less than 0.2 at.%), and the solid solubility of Sn in the Mg–Zn binary compounds is in the composition range from 0.0 to 4 ± 2 at.%.

5.2. Thermodynamic optimization

5.2.1. In–Mg system

All the experimental data discussed above were used in the present thermodynamic optimization of the In–Mg binary system. The calculated phase diagram is shown in Fig. 3 with experimental data [12,14,17–20]. In the present work, the γ' and β' phases were treated as a single fcc solution and modeled with the two sub-lattice structure of $(In, Mg)_3(In, Mg)$ as $L1_2$, and the β'' phase was modeled with a two sub-lattice structure of $(In, Mg)(In, Mg)$ as $L1_0$. The calculated peritectic reaction liquid + hcp(Mg) $\leftrightarrow \beta$ is 484 °C, which agrees well with the experimental data [14,18,19]. All the calculated invariant reactions are listed in Table 5 and are in a good agreement with the experimental data [12,14,17–20]. The calculated enthalpy of mixing of the liquid phase at 675 °C is shown in Fig. 4 along with the experimental data [22–27]. As shown in this figure, the data extrapolated from EMF measurements have large error limits compared to the experimental data obtained from direct calorimetric measurements. Consequently, in the present work, the optimization was mainly based on the experimental data [22,27] obtained by calorimetric methods. The calculated activities of Mg and In in the liquid phase at 650 °C are shown in Fig. 5 in comparison with experimental data [24,26–28]. No experimental thermodynamic data exist for intermetallic compounds. Therefore, their heat capacities were obtained with the Neumann–Kopp rule [91], with the "Zero" enthalpy of formation at 25 °C, firstly. And then the enthalpy and entropy of formation were then adjusted by fitting the phase diagram. The calculated enthalpies of formation of compounds in the In–Mg system at 25 °C are shown in the Fig. 6. All the thermodynamic parameters optimized in the present work are listed in Tables 2 and 6.

5.2.2. The In–Sn system

The calculated In–Sn binary phase diagram is shown in Fig. 7 along with experimental data [30–32,34]. The calculated temperatures of the peritectic reactions $liquid + tet \leftrightarrow \beta(InSn)$ and $liquid + bct \leftrightarrow \gamma(InSn)$ are 119 °C and 223 °C, respectively, which is in good agreement with the experimental temperature of Heumann and Alpaut [34] (120 °C and 224 °C).

The calculated enthalpy of mixing of the liquid phase at 450 °C and the calculated activity of In and Zn in the liquid at 427 °C are depicted in Figs. 7 and 8. The agreement between our calculated results and the experimental data obtained by emf and calorimetric measurements is quite good. Fig. 9 shows the calculated activity of In and Zn in the liquid phase at 427 °C along with the experimental data [37–39]. And the calculated activity of In in the solid phases at 100 °C (reference state tet(In)) is shown in Fig. 10 in comparison with the experimental data [35]. The calculated enthalpy of formation of solid phases at 100 °C is shown in Fig. 11 along with

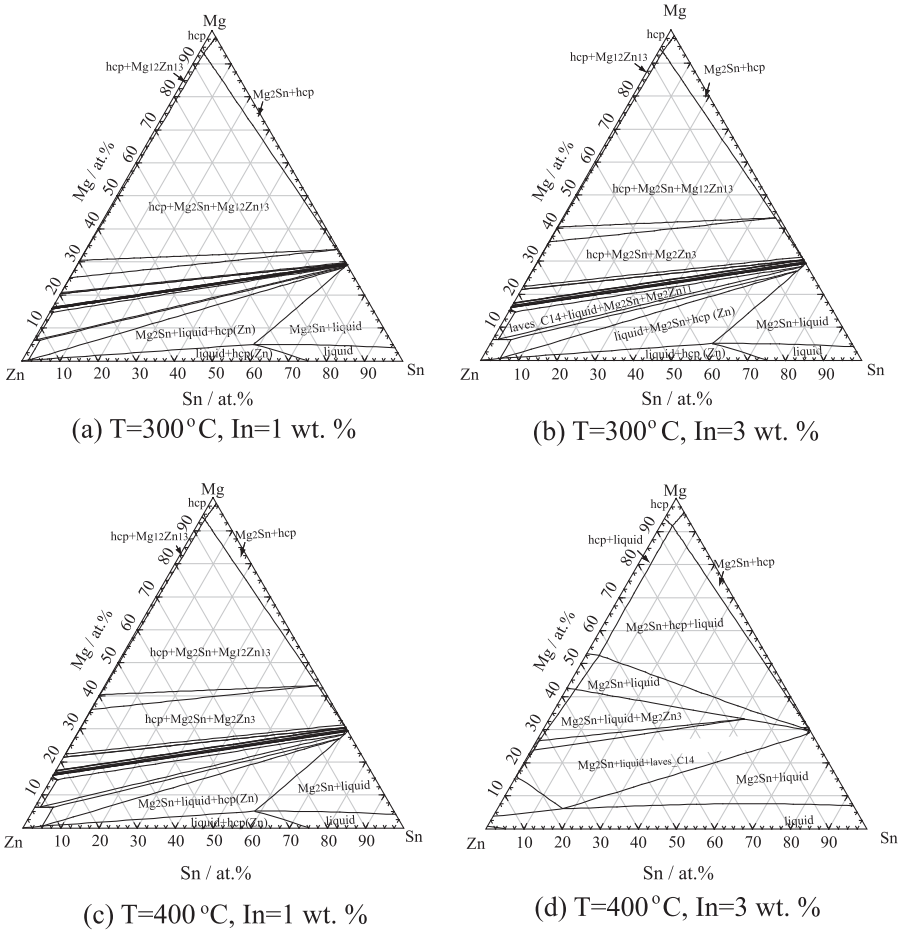

Fig. 33. Calculated isothermal sections of Mg–Sn–Zn with 1 and 3 In (wt.%) at 300 °C and 400 °C.

the experimental data [35,45]. All the thermodynamic parameters optimized in the present work are listed in Tables 2 and 6.

5.2.3. The In–Zn system

The calculated In–Zn phase diagram along with the experimental data discussed above [50–53,56] is shown in Fig. 12. The liquid phase has a tendency to form a metastable miscibility gap, which is depicted by a dotted line in Fig. 12. The consolute temperature of the miscibility gap is very close to the stable liquidus line, which was predicted by Oelsen and Zuhlke [53]. In the present work, the eutectic $liquid + tet(In) \leftrightarrow hcp(Zn)$ is calculated to lie at 144 °C and 4.5 at.% Zn, which is in reasonable agreement with experimental data [51]. The calculated enthalpy mixing of the liquid phase at 450 °C is shown in Fig. 13 along with the experimental data [52–55,58,59]. Fig. 14 shows the calculated activity of Zn in the liquid phase in the temperature range from 423 °C to 857 °C in comparison with the experimental data [52–55,60–62]. The calculated results have a good agreement with the experimental data. All the thermodynamic parameters optimized in the present work are listed in Tables 2 and 6.

5.2.4. The Mg–Sn–In ternary system

According to our experimental results, there is a very limited ternary solubility of Sn in Mg–In binary compounds, and of In in Mg_2Sn. Consequently, we assumed that there is no ternary solubility in binary compounds in the present thermodynamic optimization. The calculated isothermal sections of the Mg–Sn–In ternary system at 415 °C and 330 °C are shown in Fig. 15a and b along with the experimental data obtained in the present work. The calculated ternary isoplethal sections at 10 Sn and 5 In (at.%) are shown in Fig. 16a and b in comparison with our experimental data. The calculated phase boundaries and invariant reactions are listed in Table 3 together with our DSC experimental data. A good agreement between the calculated results and experimental data can be seen. The calculated activity of Mg in the liquid phase with the Sn/In molar ratios of 0.25, 1.00, and 0.75 versus temperature are shown in Fig. 17a–c. low Mg contents, our calculated results are in a good agreement with the experimental data of Zakulski et al. [66]. The calculated liquidus projection of the Mg–Sn–In ternary system is shown in Fig. 18. There are a total of four ternary peritectic (U type) reactions and of one ternary eutectic (E type) in the calculated Mg–Sn–In system. The calculated invariant reactions of the liquidus projection of the Mg–Sn–In ternary system are listed in Table 7. All the optimized ternary thermodynamic parameters of Mg–Sn–In ternary system in the present work are listed in Tables 2 and 6.

5.2.5. The Mg–Sn–Zn ternary system

As discussed above, there is a limited solid solubility of either Zn in Mg_2Sn or Sn in Mg–Zn binary compounds. As a result, the ternary solubility for the terminal binary compounds in the present optimization did not considered. The present calculated ternary isothermal sections at 300, 340 and 500 °C are shown in Fig. 19a–c. Other calculated isoplethal sections are depicted in Fig. 20a–l along with their related experimental data [67,69]. The calculated ternary isoplethal section at constant 10 Sn (at.%) is shown in Fig. 21 along with our DSC experimental data. The present calculations are in good agreement with all the available experimental data. The calculated liquidus projection of the Mg–Sn–Zn ternary system is shown in Fig. 22. The calculated invariant reactions in the liquidus projection of the Mg–Sn–Zn ternary system are listed in Table 8. All the ternary thermodynamic parameters optimized of Mg–Sn–Zn ternary system are listed in Tables 2 and 6.

5.2.6. The In–Sn–Zn ternary system

The calculated isoplethal sections of the In–Sn–Zn ternary system for the Sn/Zn molar ratios of 2:1, 1:1 and 1:2 are shown in Fig. 23a–c along with the experimental data reported by Xie et al. [76]. Fig. 24a–f shows the calculated isoplethal sections of the In–Sn–Zn ternary system for the In/Sn molar ratios of 5:95, 15:85, 1:2, 52:48, 2:1, and 85:15 along with the experimental data of Sabbar et al. [77]. All the present calculated results are in good agreement with the experimental data [76,77], except isoplethal section of In/Sn = 15/85 (Fig. 24b). The singals observed in the isoplethal section of In/Sn = 15/85 around 115 °C by Sabbar et al. [77] may due to the slow experimental heating/cooling rate. The calculated Scheil cooling simulations of alloys with the components of $(In15Sn85)_{1-x}Zn_x$ ($0 \leqslant x \leqslant 60$ at.%) using the present thermodynamic database show a reaction: liquid $\leftrightarrow \gamma(InSn) + \beta(InSn)$ occurring at 118 °C during the solidification process. This demonstrates that the signal reported by [77] can be due to this nonequilibrium reaction. The calculated ternary isoplethal sections at 10 In (at.%), 9 Zn (wt.%) and 6 Zn (wt.%) are shown in Fig. 25a–c in comparison with the experimental data [76,92].

The calculated mixing enthalpies of the ternary liquid phase for the In/Sn molar ratio of 1:1 and In/Zn molar ratio of 52:48 and 1:1 at various temperatures are shown in Fig. 26a and b along with experimental data [44,79,81]. The calculated partial molar enthalpy of mixing of Zn in liquid In–Sn–Zn alloys at 500 °C in comparison with the experimental data [44] is shown in Fig. 27. The calculated activity of Zn in the liquid phase (liquid standard state) for the In/Sn molar ratios of 1:3, 1:1 and 3:1 are shown in Fig. 28 along with experimental data from Nakamura et al. [80]. Fig. 29 shows the calculated activity of Zn in the liquid phase (liquid standard state) at 3 Zn (at.%) compared with the experimental data reported by Moser [78]. The calculated liquidus projection of the In–Sn–Zn ternary system is shown in Fig. 30. The calculated invariant reactions in the liquidus projection of the In–Sn–Zn ternary system are listed in Table 9. All the optimized ternary thermodynamic parameters of In–Sn–Zn ternary system in the present work are listed in Tables 2 and 6.

5.2.7. The Mg–In–Zn and Mg–Sn–In–Zn systems

No experimental phase diagram and thermodynamic data exist for the Mg–In–Zn ternary system. According to the similar Mg–Sn–In and Mg–Sn–Zn systems, one's should expect some limited ternary solubility for In in Mg–Zn binary compounds and for Zn in Mg–In binary compounds. Mg–Zn and Mg–In liquids have quite similar negative deviations from ideal mixing while In–Zn liquid has a nearly ideal mixing behavior. In the present work, the thermodynamic properties of the ternary liquid were extrapolated with the symmetric Kohler-like [88] technique within the MQMPA model. Our calculated isothermal sections of the Mg–In–Zn ternary system at 300 and 350 °C are shown in Fig. 31. The calculated liquidus projection of the Mg–In–Zn ternary system is shown in Fig. 32 and the calculated invariant reactions are listed in Table 10.

No experimental data exist for the Mg–Sn–In–Zn quaternary system. Consequently, our thermodynamic optimization was performed by extrapolating the thermodynamic parameters employed for the bounding subsystems and no additional model parameter was used. The calculated isothermal sections of Mg–Sn–Zn with 1 and 3 wt.% In at 300 °C and 400 °C are shown in Fig. 33.

6. Conclusions and discussions

Phase equilibria in the Mg-rich portion of the Mg–Sn–In ternary system at 415 °C and 330 °C, and the Mg–Sn–In ternary isoplethal sections at 10 Sn and 5 In (at.%) were investigated in the present work. No evidence of the existence of ternary compounds was

found in the present work. The present results show that the solid solubility of In in the Mg_2Sn phase and of Sn in the Mg–In binary intermetallic phases are very limited. In consideration of the high solid solubility of In in the hcp (Mg) terminal phase (Fig. 3), all the added In should dissolve into the hcp (Mg) phase upon addition to Mg–Sn alloys. A critical thermodynamic optimization of the Mg–Sn–In ternary system was carried in the present work based in part on the data obtained in the present experimental measurements. Hence, a systematic study of the relationship among the phase equilibria, the solidification process and the microstructures of the Mg–Sn based alloys with In addition can be carried out with the present thermodynamic database.

Phase equilibria in the Mg-rich portion of the Mg–Sn–Zn ternary system at 300 °C have been determined in the present work. Same as for the Mg–Sn–In ternary system, no stable ternary compound was found in this isothermal section. There is a limited solubility in all the terminal sub-binary compounds which is in agreement with the previous experimental data from Godecke and Sommer [69] and Gladyshevsky and Cherkashin [72] within the experimental error limits. The ternary isoplethal section Mg–Sn–Zn at constant 10 Sn (at.%) has been determined in the present work using DSC measurements. All the reported experimental results from previous investigators and from the present work are in a reasonable agreement. A self-consistent database of parameters of thermodynamic models for phases in the Mg–Sn–Zn ternary system was obtained in the present work after a critical evaluation of all the available experimental data. The present optimization results are in more global agreement with all the experimental data in comparison with the previous optimization performed by Meng et al. [74] using an "associate model" with the introducing of the associate or molecule of Mg_2Sn into the liquid phase. For many optimized binary systems, the optimization results are mathematically very similar with the two models of MQM and associate model. However, the associate model does not correctly predict the properties of ternary and high ordered system, which was discussed and proved by Kang and Pelton [93].

All available experimental data for the Mg–In binary system were critically evaluated. A thermodynamic optimization of the phase diagram was carried out for the first time. As shown in the previous section, the present optimization reproduces all available experimental data very well. Unfortunately, no thermodynamic data exist for the intermetallic phases and new experiments are clearly needed to fully validate the present optimized results. A critical evaluation of all available experimental data and a thermodynamic re-optimization of the Zn–In and In–Sn binary systems were carried by using the MQMPA for the liquid phase.

A self-consistent thermodynamic database for the Mg–Sn–In–Zn quaternary system has been constructed in the present work, which provides an efficient and convenient way to study and develop new Mg based alloys.

Acknowledgements

Financial supports from General Motors of Canada Ltd. and the Natural Sciences and Engineering Research Council of Canada through the CRD grant program are gratefully acknowledged. The authors would like to thank Dr. Lang Shi of Mcgill University for EMPA determination assistance, and Mr. Tian Wang and Mr. Yi-Nan Zhang of Concordia University for their help with the experiments.

References

[1] K.U. Kainer, F. Kaiser, Magnesium Alloys and Technology, Wiley Online Library, 2003.
[2] I. Polmear, Mater. Sci. Technol. Lond. 10 (1994) 1–16.
[3] X. Gao, J. Nie, Scripta Mater. 56 (2007) 645–648.
[4] M.A. Gibson, X. Fang, C.J. Bettles, C.R. Hutchinson, Scripta Mater. 63 (2010) 899–902.
[5] D.H. Kang, S.S. Park, Y.S. Oh, N.J. Kim, Mater. Sci. Eng. A 449–451 (2007) 318–321.
[6] K. Van der Planken, J. Mater. Sci. 4 (1969) 927.
[7] C.L. Mendis, C.J. Bettles, M.A. Gibson, C.R. Hutchinson, Mater. Sci. Eng. A 435–436 (2006) 163–717.
[8] C.L. Mendis, C.J. Bettles, M.A. Gibson, S. Gorsse, R. Hutchinson, Philos. Mag. Lett. 86 (2006) 443–456.
[9] A. Becerra, M. Pekguleryuz, J. Mater. Res. 24 (2009) 1722–1729.
[10] N. Saunders, A.P. Miodownik, CALPHAD (Calculation of Phase Diagrams): A Comprehensive Guide, Pergamon, 1998.
[11] H. Ohtani, K. Ishida, Thermochim. Acta 314 (1998) 69–77.
[12] W. Hume-Rothery, G.V. Raynor, J. Inst. Met. 63 (1938) 204–216.
[13] W. Hancke, Naturwissenschaften 26 (1938) 577–578.
[14] G.V. Raynor, Trans. Faraday Soc. 44 (1948) 15–28.
[15] J. Graham, G.V. Raynor, Philos. Mag. Lett. 2 (1957) 1354–1363.
[16] N. Ino, M. Hirabayashi, S. Ogawa, Trans. Jpn. Inst. Met. 6 (1965) 172–178.
[17] K. Hiraga, M. Koiwa, M. Hirabayashi, J. Less-Common Met. 15 (1968) 109–118.
[18] K.M. Pickwick, W.A. Alexander, E.H. Gamble, Can. J. Chem. 47 (1969) 3417–3427.
[19] P. Feschotte, J. Less-Common Met. 46 (1976) 51–54.
[20] Y. Watanabe, Acta Metall. 23 (1975) 691–696.
[21] A.A. Nayeb-Hashemi, J.B. Clark, Bull. Alloy Phase Diagr. 6 (1985) 149–160.
[22] K. Ehrlich, Inaugural Dissertation, Ludwig-Maximilians University, Munchen, Germany, 1965.
[23] Z. Moser, R. Castanet, EMF and calorimeteric measurements of the Mg–In liquid solutions, Czech. Conf. Calorimetry, Inst, Inorg. Chem., Czech. Acad. Sci. Prague A3 (1977) 1–4.
[24] H. Slaby, J. Terpilowski, Bull. Acad. Polon. Sco. XIII (1965) 319–322.
[25] J. Terpilowski, H. Slaby, Chem. Ann. Soc. Chim. Polon 41 (1967) 1845–1855.
[26] H. Nebell, Rev. Roum. Chim. 15 (1970) 59–65.
[27] Z. Moser, R. Castanet, Metall. Mater. Trans. B 10 (1979) 483–487.
[28] G. Chirulli, D. Ferro, V. Piacente, Thermochim. Acta 62 (1983) 171–177.
[29] B. Predel, T. Godecke, Z. Metallkd. 66 (1975) 654.
[30] D.S. Evans, A. Prince, Materials Research Society Symposium Proceeding, vol. 19, Elsevier, North-holland, 1983. p. 389.
[31] A.B. Kaplun, Phase Transformations Near the Liquidus Temperature in the Indium–Tin System, Teplofiz, Svoistva Rastvorov, 1983, pp. 65–69.
[32] Z. Wojtaszek, H. Kuzyk, Zeszyty Naukowe Uniw. Jagiellonskiego, Prace Chem. 19 (1974) 281–287.
[33] Z. Wojtaszek, H. Kuzyk, Zeszyty Naukowe Uniw. Jagiellonskiego, Prace Chem. 21 (1976) 27–32.
[34] T. Heumann, O. Alpaut, J. Less-Common Met. 6 (1964) 108–117.
[35] O. Cakir, O. Alpaut, J. Less-Common Met. 141 (1988) 11–27.
[36] B.-J. Lee, C.-S. Oh, J.-H. Shim, J. Electron. Mater. 25 (1996) 983–991.
[37] V. Vassiliev, Y. Feutelais, M. Sghaier, B. Legendre, Thermochim. Acta 315 (1998) 129–134.
[38] J. Terpilowski, E. Prezdziecka-Mycielska, Archiv. Hutnictwa 5 (1960) 281–290.
[39] D. Zivkovic, A. Mitovski, L. Balanovic, D. Manasujevic, Z. Zivkovic, J. Therm. Anal. Calorim. 102 (2010) 827–830.
[40] F.E. Wittig, P. Scheidt, Z. Phys. Chem. 28 (1961) 120–142.
[41] O.J. Kleppa, J. Phys. Chem. B 60 (1956) 842–846.
[42] A. Yazawa, T. Kawashima, K. Itagaki, Jpn. Inst. Met. 32 (1968) 1281–1287.
[43] J.P. Bros, M. Laffitte, J. Chem. Thermodyn. 2 (1970) 151–152.
[44] M. Rechchach, A. Sabbar, H. Flandorfer, H. Ipser, Thermochim. Acta 502 (2010) 66–72.
[45] O. Alpaut, T. Heumann, Acta Metall. 13 (1965) 543–548.
[46] A.D. Pelton, P. Chartrand, Metall. Mater. Trans. A 32 (2001) 1355–1360.
[47] A.D. Pelton, S.A. Degterov, G. Eriksson, C. Robelin, Y. Dessureault, Metall. Mater. Trans. B 31 (2000) 651–659.
[48] J. Dutkiewicz, W. Zakulski, Bull. Alloy Phase Diagr. 5 (1984) 284–289.
[49] C.L. Wilson, E.A. Peretti, Ind. Eng. Chem. Process Dev. 26 (1936) 204–205.
[50] V.S. Valentiner, Z. Metallkd. 35 (1943) 250–253.
[51] F.N. Rhines, A. Grobe, Trans. Metall. Soc. AIME 156 (1944) 253–262.
[52] W.T. Svirbely, S.M. Selis, J. Am. Chem. Soc. 75 (1953) 1532–1535.
[53] W. Oelsen, E.A. Zuhlke, Archiv. Eisenhuettenwesen 27 (1956) 743–752.
[54] R.W. Bohl, V.D. Hildebrandt, J. Am. Chem. Soc. 79 (1957) 2711–2727.
[55] Z. Moser, Rev. Roum. Chim. 16 (1971) 327–341.
[56] J. Dutkiewicz, Z. Moser, Bull. Acad. Polon. Sci. Technol. Sco. 31 (1983) 27.
[57] G.S. Nishimura, R.S. Fidler, M.R. Taylor, S.R. William, Can. Metall. Q. 8 (1969) 319–322.
[58] O.J. Kleppa, Acta Metall. 6 (1958) 225–232.
[59] F.E. Wittig, E. Muller, Z. Metallkd. 51 (1960) 226–238.
[60] W.G. Jung, Korean J. Mater. Res. 15 (2005) 47–54.
[61] D. Ferro, B.M. Nappi, V. Piacente, P.L. Cignini, High Temp. Sci. 10 (1978) 131–142.
[62] H. Hagiwara, S. Sugino, H. Fujiwara, Bull. Univ. Osaka 23 (1974) 41–50.
[63] B.-J. Lee, CALPHAD 20 (1996) 471–480.
[64] V. Kinzhibalo, Fazovye Rano. Metall. Splavakh 6 (1981) 73–78.
[65] Z. Moser, R. Castanet, Thermodynamic Studies on Liquid Mg–In–Sn Ternary Solutions, INKA-confi.-79-003-023, IAEA-Sm-236/35, 1979, pp. 263–271.
[66] W. Zakulski, Z. Moser, F. Sommer, J. Phase Equilib. Diffus. 18 (1997).
[67] B. Otani, J. Iron Steel Inst. Jpn. 19 (1933) 566–574.

[68] R. Agarwal, S.G. Fries, H.L. Lukas, G. Petzow, F. Sommer, T.G. Chart, G. Effenberg, Z. Metallkd. 83 (1992) 216–223.
[69] T. Godecke, F. Sommer, Z. Metallkd. 85 (1994) 683–691.
[70] M. Mingolo, B. Arcondo, E. Nassif, H. Sirkin, Z. Naturforsch. A A41 (1986) 1357–1360.
[71] H. Sirkin, N. Mingolo, E. Nassif, B. Arcondo, J. Non-Cryst. Solids 93 (1987) 323–330.
[72] E.I. Gladyshevsky, E.E. Cherkashin, Zh. Neorg. Khim. 1 (1959) 1394–1401.
[73] P. Ghosh, M.D. Mezbahul-Islam, M. Medraj, CALPHAD 36 (2012) 28–43.
[74] F. Meng, J. Wang, L. Liu, Z. Jin, J. Alloys Comp. 508 (2010) 570–581.
[75] S.W. Yoon, J.R. Soh, H.M. Lee, B.-J. Lee, Acta Mater. 45 (1997) 951–960.
[76] Y. Xie, H. Schicketanz, A. Mikura, Bericht. Bunsenges. Phys. Chem. 102 (1998) 1334–1338.
[77] A. Sabbar, A. Zrineh, M. Gambino, J.P. Bros, B. Arcondo, Thermochim. Acta 369 (2001).
[78] Z. Moser, Z. Metallkd. 65 (1974) 106–111.
[79] J.M. Fiorani, C. Naguet, J. Hertz, A. Bourkba, L. Bouirden, Z. Metallkd. 88 (1997) 711.
[80] Y. Nakamura, M. Shimoji, K. Niwa, Trans. Jpn. Inst. Met. 5 (1964) 28–32.
[81] P. Anres, M. Alaoui-elbelghiti, M. Gambino, J.P. Bros, Thermochim. Acta 346 (2000) 49–56.
[82] Y. Xie, Z.Y. Qiao, A. Mikula, CALPHAD 25 (2001) 3–10.
[83] Y. Cui, X.J. Liu, I. Ohnuma, R. Kainuma, H. Ohtani, K. Ishida, J. Alloys Comp. 320 (2001) 234–241.
[84] C.W. Bale, P. Chartrand, S.A. Degterov, G. Eriksson, K. Hack, R. Ben Mahfoud, J. Melancon, A.D. Pelton, S. Petersen, CALPHAD 26 (2002) 189–228.
[85] I.-H. Jung, D.H. Kang, W.J. Park, N.J. Kim, S.H. Ahn, CALPHAD 31 (2007) 192–200.
[86] P.J. Spencer, Mg–Zn system, database, CRCT (Ed.), Montreal, 2006.
[87] Y.-B. Kang, A.D. Pelton, P. Chartrand, C.D. Fuerst, CALPHAD 32 (2008) 413–422.
[88] A.D. Pelton, CALPHAD 25 (2001) 319–328.
[89] M. Hillert, J. Alloys Comp. 320 (2001) 161–176.
[90] A.T. Dinsdale, CALPHAD 15 (1991) 317–425.
[91] H. Kopp, Philos. Trans. Roy. Soc. A 155 (1865) 71–202.
[92] S.W. Yoon, J.R. Soh, B.J. Lee, H.M. Lee, Design and reliability of solders and solders interconnections, in: R.K. Mahidhara, D.R. Frear, S.M.L. Saty, K.L. Murty, P.K. Liaw, W. Winterbottom (Eds.), J. Min. Met. Mater. Soc., 1997, p. 121.
[93] Y.-B. Kang, A.D. Pelton, CALPHAD 34 (2010) 180–188.